ACS EARTH AND SPACE CHEMISTRY

http://pubs.acs.org/journal/aesccq

Article

Density Functional Theory Calculations of Equilibrium Mo Isotope Fractionation Factors among $MoO_xS_{4-x}^{2-}$ Species in the Aqueous Phase by the ONIOM Method

Yuyang He,*,# Caihong Gao,# Wei Wei, and Yun Liu

Cite This: ACS Earth Space Chem. 2023, 7, 142−155

Read Online

ACCESS | Metrics & More | Article Recommendations | Supporting Information

ABSTRACT: Molybdenum (Mo) is a redox-sensitive metal element. Its isotope composition (δ^{98}Mo) has the potential to reconstruct oceanic oxygenation extent in deep time. To accurately reconstruct the bulk δ^{98}Mo value of ancient seawater from sediment records, it is necessary to clarify the Mo isotope fractionation mechanism during the transformation among thiomolybdates ($MoO_xS_{4-x}^{2-}$, x = 0∼4) in marine environments. For aqueous systems, predicting the equilibrium isotope fractionation factors theoretically needs careful treatment of solvent effects. The commonly used water-droplet or periodical boundary condition methods are not only troublesome but also time-consuming. We test the efficiency of the two-layer own N-layer integrated molecular orbital molecular mechanics (ONIOM) method in predicting the reduced partition function ratios (β factors) of the $MoO_xS_4^{2-}$ species in aqueous phases. Compared to other methods, the ONIOM method can produce β factors with the same accuracy and considerably fewer computational resources. The predicted β factors are in the order $MoO_{4(aq)}^{2-}$ > $MoO_3S_{(aq)}^{2-}$ > $MoO_2S_{2(aq)}^{2-}$ > $MoOS_{3(aq)}^{2-}$ > $MoS_{4(aq)}^{2-}$, which are in line with previous laboratory experiments and field observations. The new results provide the basic data for reconstructing δ^{98}Mo values in suboxic, ferruginous, and weakly euxinic sediments.

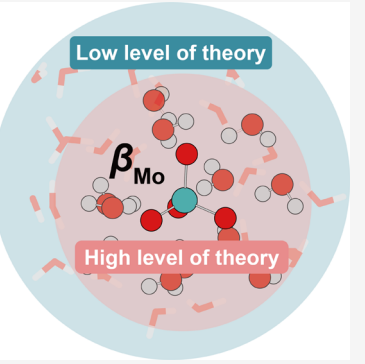

KEYWORDS: *paleoredox proxy, ab initio molecular dynamics, implicit solvent model, dispersion correction, water-droplet, periodical boundary condition*

1. INTRODUCTION

Molybdenum (Mo) isotopes have been used as a paleo-oxybarometer to reconstruct global marine redox evolutions throughout the Earth's history.[1−5] Such applications are based on the distinct Mo isotope fractionations during the transformation of Mo species and the removal of Mo from seawater under different redox conditions.[6−9] The speciation, reactivity, and solubility of Mo species are controlled by the redox condition of ambient water.[10,11] Molybdate (MoO_4^{2-}) exists dominantly in an oxic environment. In a euxinic environment, MoO_4^{2-} exchanges ligands with H_2S-bearing systems and forms thiomolybdates ($MoO_xS_{4-x}^{2-}$, x = 0∼4) in the following order[12]

$$MoO_4^{2-} \rightarrow MoO_3S^{2-} \rightarrow MoO_2S_2^{2-} \rightarrow MoOS_3^{2-} \rightarrow MoS_4^{2-}$$

(mono-) → (di-) → (tri-) → (tetra-) thiomolybdate

Under a euxinic condition with pH = ∼8, the thiolation rate of dissolved Mo species from left to right is ∼5 h, ∼50 h, ∼60 days, and ∼1.5 years, respectively.[13,14] Higher H_2S concentrations, lower pH, and more microbial activities can accelerate the thiolation processes.[14−16] Mo isotopes fractionate during species transformation, which can characterize the defined process.[17,18]

Most previous research studies focus on the isotope fractionation factors (α) of sequestration processes since the conversion from molybdate to thiomolybdate was assumed to be stoichiometric.[17] The assumption has been challenged. First, it has been observed that in a water column, the most abundant Mo species changes with depth from MoO_4^{2-} to MoO_3S^{2-} and $MoO_2S_2^{2-}$ to $MoOS_3^{2-}$ and MoS_4^{2-}.[7,11] The transformation from chemically unreactive molybdate to highly reactive thiomolybdate has been proposed to be the prime reason for authigenic Mo enrichment in sediments[10,11,19] and a reason for a lighter δ^{98}Mo value in euxinic sediments.[20−23] Second, in suboxic, ferruginous, and weakly euxinic settings where H_2S concentrations are between 0.1 and 11 μmol/L, thiolation of molybdate is slow or incomplete. The intermediate thiomolybdate species coexist, and the sequestration may occur nonquantitatively.[7,12,14,24] Therefore, clarifying the α factors among the $MoO_xS_{4-x}^{2-}$ species is the first step toward quantifying the dynamics of intermediate thiomolyb-

Received: September 1, 2022
Revised: November 22, 2022
Accepted: November 28, 2022
Published: December 13, 2022

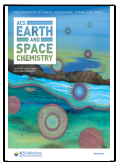

https://doi.org/10.1021/acsearthspacechem.2c00268
ACS Earth Space Chem. 2023, 7, 142−155

date species and establishing a reliable Mo isotope paleoredox proxy.

Density function theory (DFT) calculation combined with the Urey−Bigeleisen−Goeppert-Mayer (U−B−GM) model[25,26] is an efficient and reliable method to predict equilibrium isotope fractionation factors (α_{eq}) due to its good predictions on harmonic vibrational frequencies.[27−29] Currently, only one study calculated the α_{eq} values among MoO_4^{2-}, $MoO_2S_2^{2-}$, and MoS_4^{2-} by isolated molecule models with the implicit solvent effect.[17] Such practice may mismatch the observations in ocean water and laboratory experiments since the solvent molecules around the solute deeply influence the chemical behaviors of compounds.[27−35] To properly address the solvent effects in theoretical calculations, a hybrid-solvent model, which includes implicit and explicit solvent effects, as well as dispersion correction, is needed. Water-droplet[27−35] and periodic boundary condition (PBC)[36−38] methods are usually used to deal with aqueous phases with the consideration of explicit solvent molecules. Nevertheless, such methods are labor-intensive and require large amounts of computational resources. The own N-layer integrated molecular orbital molecular mechanics (ONIOM) method has been used to simplify the geometry and energy calculations of big systems by treating different layers with different methods.[36] Theoretically, it should also work in predicting α_{eq} factors of aqueous systems.

In this work, we evaluate the influences of implicit and explicit solvent effects, as well as dispersion correction on the predicted α_{eq} values of thiomolybdates first. Then, we test the robustness and efficiency of the ONIOM method in predicting α_{eq} factors for the aqueous phase. Using the predicted α_{eq} factors for $MoO_xS_{4-x}^{2-}$ species in the aqueous phase, we retrospect and prospect the application of Mo isotope compositions and proposed essentials for constructing a reliable quantitative paleoredox proxy.

2. METHODS

2.1. Equilibrium Isotope Fractionation Theory. The Mo isotope composition was initially expressed as $\delta^{97}Mo = [(^{97}Mo/^{95}Mo)_{sample}/(^{97}Mo/^{95}Mo)_{standard} - 1]$.[6,37] Therefore, the calculated α_{eq} factors have been reported as $^{97/95}\alpha_{eq}$.[17,38−41] With the development of the $^{97}Mo-^{100}Mo$ double-spike analysis technique,[42] the following measurements reported the Mo isotope composition as $\delta^{98}Mo$.[9,18,43−45] The $\delta^{97}Mo$ and $\delta^{98}Mo$ values can be converted to each other by a geometric rule: $\delta^{97}Mo \approx 2/3 \times \delta^{98}Mo$ and so do the $^{97/95}\alpha$ and $^{98/95}\alpha$ values. To be consistent with recent works, here we report the Mo isotope fractionation factor as $^{98/95}\alpha$, and all the $^{97/95}\alpha$ values in the literature are converted to $^{98/95}\alpha$ values unless specified.

The equilibrium isotope fractionation theory is used to calculate the Mo isotope fractionation factors. An isotope exchange reaction between species A and B can be expressed as:

$$A + B^* \rightleftharpoons A^* + B$$

where the species with * contain the rare isotope (i.e., ^{98}Mo in this case) and the ones without * contain the most abundant isotope (i.e., ^{95}Mo in this case).

The α_{eq} factor between A and B can be expressed as the ratio of their reduced partition function ratio (β factor) that is the α_{eq} factor between an atom in a specific bond environment and its atomic form

$$\alpha_{eq(A-B)} = \frac{\beta_A}{\beta_B} \quad (1)$$

in which the β factors can be estimated in harmonic approximation[46−48] using the U−B−GM model[25,26]

$$\beta = \prod_i^N \left(\frac{u_i^*}{u_i}\right)\left(\frac{e^{-u_i^*/2}}{e^{-u_i/2}}\right)\left(\frac{1-e^{-u_i}}{1-e^{-u_i^*}}\right) \quad (2)$$

$$u = \frac{h\upsilon}{k_B T} \quad (3)$$

where N denotes the number of the harmonic vibrational modes (for nonlinear molecules, $N = 3n-6$; for linear molecules, $N = 3n-5$; n is the number of atoms), h is the Planck constant, ν is the harmonic vibration frequency, k_B is the Boltzmann constant, and T is the temperature in Kelvin.

A uniform scale factor is usually used to scale the theoretical frequencies to the experimental values. However, as previous work suggested, the frequencies needed in the U−B−GM model are harmonic, and manually scaling the frequencies may introduce errors to the predicted β factors.[49] In addition, the influences of the scale factors are mostly canceled out in the reported α values.[33,34,50−52] Thus, no scale factors were used in the current work.

For better illustration, the α and β values are often reported in the form of $\ln\alpha$ and $\ln\beta$ values in per mil (‰).

2.2. Computational Details. DFT calculations were used to optimize structures and calculate harmonic vibrational frequencies. The isolated molecules, water-droplet, and ONIOM calculations were performed using the software Gaussian 16.[53] The PBC calculations were performed using the Vienna ab initio simulation package (VASP).[54] In this work, "*g*" denotes isolated molecules in the gaseous phase, "*i*" denotes isolated molecules with the implicit solvent effect integral-equation-formalism polarizable continuum model (IEFPCM),[55] "aq-w" denotes the aqueous phase by the water-droplet method, "aq-p" denotes the aqueous phase by the PBC method, and "aq-o" denotes the aqueous phase by the ONIOM method.

2.2.1. Water-Droplet Method. The water-droplet or supermolecule explicit solvent method introduces solvent molecules to simulate a solution environment more realistically, which has been used to calculate β values of species in the aqueous phase.[27−35] We performed the water-droplet method on MoO_4^{2-}, MoS_4^{2-}, Na_2MoO_4, and Na_2MoS_4. The procedure is to add six water molecules to a system and optimize the structure repeatedly until the average β value converges. All structures were optimized to the local energy minimum with no imaginary frequency. The optimized structure of each configuration has the target species at the center of the water cluster. To better sample the structures of liquids, we built four independent water-droplet models with different initial configurations for each species. The final β values were taken as the average of the last eight configurations (with 24 and 30 water molecules). More details of the water-droplet method can be found in our previous works.[33−35]

The B3LYP exchange−correlation functional[56,57] was used to optimize geometries and calculate vibrational frequencies. The LANL2DZ-ECP basis set[58,59] was used for Mo atoms, and

https://doi.org/10.1021/acsearthspacechem.2c00268
ACS Earth Space Chem. 2023, 7, 142−155

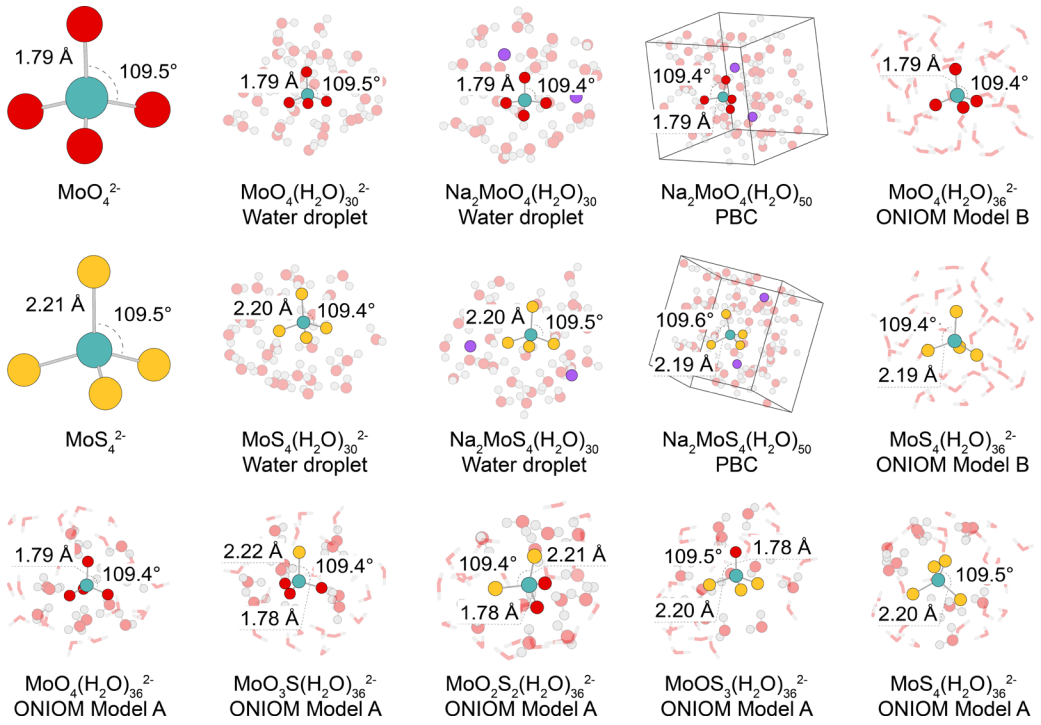

Figure 1. Optimized representative configurations and selected geometry parameters. Gray, red, purple, yellow, and green represent H, O, Na, S, and Mo atoms, respectively. Ball-and-stick models were calculated at the high theoretical level, and tube models were calculated at the low theoretical level. Gray cubic boxes in the PBC models denote periodical boundaries.

the 6-311+g(2df,p) basis set[60,61] was used for H, O, Na, and S atoms.

The IEFPCM was used for the implicit solvent effect. The dispersion effect was considered according to the D3 dispersion correction with Becke−Jonson damping (GD3BJ).[62,63] To test the influences of the IEFPCM and D3 dispersion correction, we calculated $MoO_4(H_2O)_{30}^{2-}$_B and $MoS_4(H_2O)_{30}^{2-}$_B models without IEFPCM and D3 dispersion correction (the explicit model), with IEFPCM but without D3 dispersion correction (the explicit + IEFPCM model), and without IEFPCM but with D3 dispersion correction (the explicit + D3 model).

2.2.2. PBC Method. The PBC method models an infinite or semi-infinite domain using its supercell, which was performed to predict the β factors of Na_2MoO_4 and Na_2MoS_4 in the aqueous phase. First, the solute molecule and 50 water molecules were put into a cubic box. The unit-cell parameters were set as 11.50 Å to ensure that the densities are close to 1 g/cm^3, and the statistical pressure is close to zero. Then, first-principles molecular dynamics (FPMD) simulations were performed based on the canonical ensemble (NVT) with the Nose thermostat. We applied the projector augmented wave method and the Perdew, Burke, and Ernzerhof generalized gradient approximation[64] for the exchange−correlation functional. The plane-wave energy cutoff was set as 600 eV with a 1 × 1 × 1 k-point grid. With the time step of 1 fs, we performed the FPMD simulations at 300 K for 20 ps to let the systems reach equilibrium, and then the simulations were run for at least 30 ps to generate the FPMD trajectories. Four snapshots were randomly extracted from the trajectories of each system. The atomic positions of the extracted configurations were optimized with the force convergence criteria of 10^{-3} eV/Å. After optimization, the vibrational frequencies were calculated with the finite displacement method.[65]

2.2.3. ONIOM Method. The main idea of the ONIOM method is to divide the entire system into multiple layers, with a small but important part of the system described by expensive quantum mechanics (QM) methods and the rest of the system described by lower theoretical levels.[66] The center layer was defined as the "model" system and treated with both "high" and "low" levels of calculation. The entire "real" system was treated only at the "low" level of calculation. The ONIOM energy is defined as

$$E(\text{ONIOM}) = E(\text{high, model}) + E(\text{low, real}) - E(\text{low, model})$$

The ONIOM models can reproduce the geometries and the reaction energies of the full QM models with considerably fewer computational resources,[67,68] which have been used to include explicit solvent molecules in calculations.[69−71] In the present work, we calculated the solution systems by a two-layer ONIOM(QM/QM) method.

To sample initial structures for ONIOM models, we used the atom-centered density matrix propagation (ADMP) MD simulation[72−74] on the structures of Mo species in 90-water-molecule clusters. Since the results of the ADMP simulations were only used as the initial structure of further calculation, here we performed the ADMP simulation with a semiempirical calculation method, the PM6 Hamiltonian,[75] at 325 K for 10 ps with a time step of 0.5 fs. Ten configurations were randomly chosen from the last 5 ps trajectories of each Mo species, and clusters with the 36 water molecules nearest to the Mo species were cut for further calculation. The script for cutting a cluster with specific numbers of water molecules can be found in the Supporting Information.

To test the influences of different explicit solvent molecule treatments on the calculated β and α values, here we used the

https://doi.org/10.1021/acsearthspacechem.2c00268
ACS Earth Space Chem. 2023, 7, 142−155

Table 1. Selected Geometric Parameters of Different Models (d: Distances in Å, ∠: Angles in °)[a]

model	method	d_{Mo-O}	d_{Mo-S}	∠X−Mo−X
MoO_4^{2-}	gaseous	1.79 ± 0.00		109.5 ± 0.0
MoO_4^{2-}	IEFPCM	1.79 ± 0.00		109.5 ± 0.0
$MoO_4(H_2O)_{30}^{2-}$	water-droplet	1.79 ± 0.01		109.5 ± 1.7
$Na_2MoO_4(H_2O)_{30}$	water-droplet	1.79 ± 0.02		109.4 ± 1.6
$Na_2MoO_4(H_2O)_{50}$	PBC	1.79 ± 0.03		109.4 ± 3.2
$MoO_4(H_2O)_{36}^{2-}$	ONIOM model A	1.79 ± 0.01		109.4 ± 3.0
$MoO_4(H_2O)_{36}^{2-}$	ONIOM model B	1.79 ± 0.01		109.4 ± 2.9
MoS_4^{2-}	gaseous		2.21 ± 0.00	109.5 ± 0.0
MoS_4^{2-}	IEFPCM		2.21 ± 0.00	109.5 ± 0.0
$MoS_4(H_2O)_{30}^{2-}$	water-droplet		2.20 ± 0.01	109.4 ± 1.4
$Na_2MoS_4(H_2O)_{30}$	water-droplet		2.20 ± 0.02	109.5 ± 1.5
$Na_2MoS_4(H_2O)_{50}$	PBC		2.19 ± 0.03	109.6 ± 1.1
$MoS_4(H_2O)_{36}^{2-}$	ONIOM model A		2.20 ± 0.03	109.5 ± 2.0
$MoS_4(H_2O)_{36}^{2-}$	ONIOM model B		2.19 ± 0.03	109.5 ± 2.0
$MoO_3S(H_2O)_{36}^{2-}$	ONIOM model A	1.78 ± 0.01	2.22 ± 0.02	109.4 ± 2.3
$MoO_2S_2(H_2O)_{36}^{2-}$	ONIOM model A	1.78 ± 0.01	2.21 ± 0.03	109.4 ± 2.3
$MoOS_3(H_2O)_{36}^{2-}$	ONIOM model A	1.78 ± 0.01	2.20 ± 0.03	109.5 ± 1.7

[a]Note: For the isolated molecules, the data are the mean values of four bonds or six angles. For the PBC and ONIOM models, the data are the mean values of all bonds and angles in 4 and 10 configurations, respectively. For the water-droplet models, the data are the mean values of all bonds or angles in four configurations with 30 explicit water molecules. The "X" in "∠X−Mo−X" represents O or S.

ONIOM model on MoO_4^{2-} and MoS_4^{2-} ions with two different ways of defining layers. In model A, the Mo species and the water molecules that form hydrogen bonds with the solute molecules were defined as the model systems. The numbers of water molecules in the model systems are between 9 and 14 (Table S1). In model B, only the Mo species were defined as the model system. Models A and B with the same index share the same initial structure. A high-level calculation was performed at the B3LYP/(6-311+G(2df,p), LANL2DZ) level with IEFPCM, which was the same as the water-droplet models, and a low-level calculation was performed at the B3LYP/(6-31G, LANL2DZ) level with ONIOM-PCM/X.[36] The D3 dispersion correction was also considered in the calculations.

After a careful evaluation, the ONIOM model A is chosen as the most effective and efficient method for the calculation of aqueous systems. Thus, we calculated the β values of $MoO_3S_{(aq)}^{2-}$, $MoO_2S_{2(aq)}^{2-}$, and $MoOS_{3(aq)}^{2-}$ by ONIOM model A.

3. RESULTS

3.1. Geometry Parameters. The optimized geometries for the isolated molecules and the representative configurations of aqueous phases are presented in Figure 1. The selected geometry parameters for all models are listed in Table 1. The optimized structure coordinates and detailed geometry parameters can be found in Tables S2−S5.

For the gaseous phases, our calculations yield 1.79 Å for the Mo−O bond (d_{Mo-O}) and 109.5° for the ∠O−Mo−O angle of MoO_4^{2-}, and 2.21 Å for the Mo−S bond (d_{Mo-S}) and 109.5° for the ∠S−Mo−S angle of MoS_4^{2-}. The results of the IEFPCM models are the same as the gaseous phases. The geometries of water-droplet models are similar to the isolated molecules, with d_{Mo-O} = 1.79 ± 0.01 Å and ∠O−Mo−O = 109.4 ± 1.7° for $MoO_4(H_2O)_{30}^{2-}$ and d_{Mo-S} = 2.20 ± 0.01 Å and ∠S−Mo−S = 109.5 ± 1.4° for $MoS_4(H_2O)_{30}^{2-}$. In the water-droplet models, Na^+ ion has little influence on the geometries, with d_{Mo-O} = 1.79 ± 0.02 Å and ∠O−Mo−O = 109.4 ± 1.6° for $Na_2MoO_4(H_2O)_{30}$ and d_{Mo-S} = 2.20 ± 0.02 Å and ∠S−Mo−S = 109.4 ± 1.5° for $Na_2MoS_4(H_2O)_{30}$. The PBC models also produce similar optimized geometries, with d_{Mo-O} = 1.79 ± 0.03 Å and ∠O−Mo−O = 109.4 ± 3.2° for $Na_2MoO_4(H_2O)_{50}$ and d_{Mo-S} = 2.19 ± 0.03 Å and ∠S−Mo−S = 109.6 ± 1.1° for $Na_2MoS_4(H_2O)_{50}$. The optimized geometries of the ONIOM models are similar to the results of the other models. The ONIOM model A estimates d_{Mo-O} = 1.79 ± 0.02 Å and ∠O−Mo−O = 109.4° ± 3.0° for $MoO_4(H_2O)_{36}^{2-}$ and d_{Mo-S} = 2.20 ± 0.03 Å and ∠S−Mo−S = 109.5 ± 2.0° for $MoS_4(H_2O)_{36}^{2-}$. The ONIOM model B estimates d_{Mo-O} = 1.79 ± 0.01 Å and ∠O−Mo−O = 109.4 ± 2.9° for $MoO_4(H_2O)_{36}^{2-}$ and d_{Mo-S} = 2.19 ± 0.03 Å and ∠S−Mo−S = 109.5 ± 2.0° for $MoS_4(H_2O)_{36}^{2-}$.

The results of d_{Mo-O} in MoO_4^{2-} are consistent with previous experimental and theoretical calculation results, for example, 1.78 Å for MoO_4^{2-} in solution determined by K-edge extended XAFS,[76] 1.794 Å for gaseous MoO_4^{2-} calculated by the DFT method at the polarized SBK/B3LYP level and polarized SBK/CCSD level,[17] and 1.79 Å for MoO_4^{2-} with 12 explicit water molecules calculated by the DFT method at the B3LYP/(6−311+G(2df,p), LANL2DZ) level.[41] The results of d_{Mo-S} in MoS_4^{2-} are consistent with previous experimental and theoretical calculation results, for example, 2.178 Å for MoS_4^{2-} in solution determined by electronic absorption spectra[77] and 2.21−2.29 Å for gaseous MoS_4^{2-} calculated by various levels of DFT combined with a variety of basis sets.[78] Both MoO_4^{2-} and MoS_4^{2-} are tetrahedrons; thus, the ∠O−Mo−O of MoO_4^{2-} and ∠S−Mo−S of MoS_4^{2-} are 109.4−109.5°, which are consistent with the DFT calculation results of MoS_4^{2-}.[78] Our calculation results indicate that the ONIOM method can accurately predict the geometries of the aqueous systems.

The optimized structures of $MoO_3S(H_2O)_{36}^{2-}$, $MoO_2S_2(H_2O)_{36}^{2-}$, and $MoOS_3(H_2O)_{36}^{2-}$ of the ONIOM model A are also tetrahedrons with ∠X−Mo−X = 109.4−109.5°, where X represents O or S. For $MoO_3S(H_2O)_{36}^{2-}$, d_{Mo-O} = 1.78 ± 0.01 Å and d_{Mo-S} = 2.22 ± 0.02 Å. For $MoO_2S_2(H_2O)_{36}^{2-}$, d_{Mo-O} = 1.78 ± 0.01 Å and d_{Mo-S} = 2.21 ±

https://doi.org/10.1021/acsearthspacechem.2c00268
ACS Earth Space Chem. 2023, 7, 142−155

Table 2. Calculated $\beta_{aq\text{-}w}$ Values for $MoO_4(H_2O)_n^{2-}$, $MoS_4(H_2O)_n^{2-}$, $Na_2MoO_4(H_2O)_n$, and $Na_2MoS_4(H_2O)_n$ at 25 °C by the Water-Droplet Method

model	β	model	β	model	β	model	β
$MoO_4(H_2O)_6^{2-}$_A	1.0119	$MoS_4(H_2O)_6^{2-}$_A	1.0068	$Na_2MoO_4(H_2O)_6$_A	1.0120	$Na_2MoS_4(H_2O)_6$_A	1.0068
$MoO_4(H_2O)_6^{2-}$_B	1.0120	$MoS_4(H_2O)_6^{2-}$_B	1.0068	$Na_2MoO_4(H_2O)_6$_B	1.0121	$Na_2MoS_4(H_2O)_6$_B	1.0066
$MoO_4(H_2O)_6^{2-}$_C	1.0119	$MoS_4(H_2O)_6^{2-}$_C	1.0067	$Na_2MoO_4(H_2O)_6$_C	1.0120	$Na_2MoS_4(H_2O)_6$_C	1.0069
$MoO_4(H_2O)_6^{2-}$_D	1.0120	$MoS_4(H_2O)_6^{2-}$_D	1.0067	$Na_2MoO_4(H_2O)_6$_D	1.0121	$Na_2MoS_4(H_2O)_6$_D	1.0069
average[a]	**1.0120 ± 0.0001**		**1.0068 ± 0.0001**		**1.0121 ± 0.0001**		**1.0068 ± 0.0001**
$MoO_4(H_2O)_{12}^{2-}$_A	1.0123	$MoS_4(H_2O)_{12}^{2-}$_A	1.0069	$Na_2MoO_4(H_2O)_{12}$_A	1.0121	$Na_2MoS_4(H_2O)_{12}$_A	1.0068
$MoO_4(H_2O)_{12}^{2-}$_B	1.0124	$MoS_4(H_2O)_{12}^{2-}$_B	1.0068	$Na_2MoO_4(H_2O)_{12}$_B	1.0123	$Na_2MoS_4(H_2O)_{12}$_B	1.0070
$MoO_4(H_2O)_{12}^{2-}$_C	1.0121	$MoS_4(H_2O)_{12}^{2-}$_C	1.0070	$Na_2MoO_4(H_2O)_{12}$_C	1.0123	$Na_2MoS_4(H_2O)_{12}$_C	1.0069
$MoO_4(H_2O)_{12}^{2-}$_D	1.0120	$MoS_4(H_2O)_{12}^{2-}$_D	1.0068	$Na_2MoO_4(H_2O)_{12}$_D	1.0122	$Na_2MoS_4(H_2O)_{12}$_D	1.0069
average	**1.0122 ± 0.0002**		**1.0069 ± 0.0001**		**1.0122 ± 0.0001**		**1.0069 ± 0.0001**
$MoO_4(H_2O)_{18}^{2-}$_A	1.0123	$MoS_4(H_2O)_{18}^{2-}$_A	1.0070	$Na_2MoO_4(H_2O)_{18}$_A	1.0122	$Na_2MoS_4(H_2O)_{18}$_A	1.0069
$MoO_4(H_2O)_{18}^{2-}$_B	1.0125	$MoS_4(H_2O)_{18}^{2-}$_B	1.0069	$Na_2MoO_4(H_2O)_{18}$_B	1.0122	$Na_2MoS_4(H_2O)_{18}$_B	1.0070
$MoO_4(H_2O)_{18}^{2-}$_C	1.0122	$MoS_4(H_2O)_{18}^{2-}$_C	1.0068	$Na_2MoO_4(H_2O)_{18}$_C	1.0121	$Na_2MoS_4(H_2O)_{18}$_C	1.0070
$MoO_4(H_2O)_{18}^{2-}$_D	1.0123	$MoS_4(H_2O)_{18}^{2-}$_D	1.0068	$Na_2MoO_4(H_2O)_{18}$_D	1.0122	$Na_2MoS_4(H_2O)_{18}$_D	1.0069
average	**1.0123 ± 0.0001**		**1.0069 ± 0.0001**		**1.0122 ± 0.0000**		**1.0070 ± 0.0001**
$MoO_4(H_2O)_{24}^{2-}$_A	1.0125	$MoS_4(H_2O)_{24}^{2-}$_A	1.0071	$Na_2MoO_4(H_2O)_{24}$_A	1.0122	$Na_2MoS_4(H_2O)_{24}$_A	1.0071
$MoO_4(H_2O)_{24}^{2-}$_B	1.0122	$MoS_4(H_2O)_{24}^{2-}$_B	1.0070	$Na_2MoO_4(H_2O)_{24}$_B	1.0122	$Na_2MoS_4(H_2O)_{24}$_B	1.0070
$MoO_4(H_2O)_{24}^{2-}$_C	1.0122	$MoS_4(H_2O)_{24}^{2-}$_C	1.0070	$Na_2MoO_4(H_2O)_{24}$_C	1.0123	$Na_2MoS_4(H_2O)_{24}$_C	1.0070
$MoO_4(H_2O)_{24}^{2-}$_D	1.0123	$MoS_4(H_2O)_{24}^{2-}$_D	1.0071	$Na_2MoO_4(H_2O)_{24}$_D	1.0122	$Na_2MoS_4(H_2O)_{24}$_D	1.0070
average	**1.0123 ± 0.0001**		**1.0071 ± 0.0001**		**1.0122 ± 0.0001**		**1.0070 ± 0.0001**
$MoO_4(H_2O)_{30}^{2-}$_A	1.0123	$MoS_4(H_2O)_{30}^{2-}$_A	1.0070	$Na_2MoO_4(H_2O)_{30}$_A	1.0125	$Na_2MoS_4(H_2O)_{30}$_A	1.0072
$MoO_4(H_2O)_{30}^{2-}$_B	1.0123	$MoS_4(H_2O)_{30}^{2-}$_B	1.0070	$Na_2MoO_4(H_2O)_{30}$_B	1.0122	$Na_2MoS_4(H_2O)_{30}$_B	1.0071
$MoO_4(H_2O)_{30}^{2-}$_C	1.0122	$MoS_4(H_2O)_{30}^{2-}$_C	1.0072	$Na_2MoO_4(H_2O)_{30}$_C	1.0123	$Na_2MoS_4(H_2O)_{30}$_C	1.0073
$MoO_4(H_2O)_{30}^{2-}$_D	1.0125	$MoS_4(H_2O)_{30}^{2-}$_D	1.0073	$Na_2MoO_4(H_2O)_{30}$_D	1.0122	$Na_2MoS_4(H_2O)_{30}$_D	1.0071
average	**1.0123 ± 0.0001**		**1.0071 ± 0.0002**		**1.0123 ± 0.0001**		**1.0072 ± 0.0001**
preferred value[b]	**1.0123**		**1.0071**		**1.0123**		**1.0071**
ln β (‰)	**12.2**		**7.1**		**12.2**		**7.1**

[a]The "average" data in bold are the mean values of four clusters (i.e., clusters A, B, C, and D) of the same calculation settings. [b]The "preferred value" is the recommended β values in the aqueous phase, which are mean values of eight clusters with 24 and 30 water molecules.

https://doi.org/10.1021/acsearthspacechem.2c00268
ACS Earth Space Chem. 2023, 7, 142−155

Table 3. Calculated $\beta_{aq\text{-}p}$ Values for $Na_2MoO_4(H_2O)_{50}$ and $Na_2MoS_4(H_2O)_{50}$ at 25 °C by the PBC Method

model	β	model	β
$Na_2MoO_4(H_2O)_{50}$_A	1.0123	$Na_2MoS_4(H_2O)_{50}$_A	1.0072
$Na_2MoO_4(H_2O)_{50}$_B	1.0123	$Na_2MoS_4(H_2O)_{50}$_B	1.0073
$Na_2MoO_4(H_2O)_{50}$_C	1.0123	$Na_2MoS_4(H_2O)_{50}$_C	1.0073
$Na_2MoO_4(H_2O)_{50}$_D	1.0123	$Na_2MoS_4(H_2O)_{50}$_D	1.0073
average[a]	1.0123 ± 0.0000		1.0073 ± 0.0000
lnβ(‰)	**12.2**		**7.3**

[a]The "average" data in bold are the mean values of four configurations of the same calculation settings.

Table 4. Calculated $\beta_{aq\text{-}o}$ Values for $MoO_4(H_2O)_{36}^{2-}$ and $MoS_4(H_2O)_{36}^{2-}$ at 25 °C by the Two ONIOM Models

model A[a]	β	model A	β	model B[b]	β	model B	β
$MoO_4(H_2O)_{36}^{2-}$_A	1.0122	$MoS_4(H_2O)_{36}^{2-}$_A	1.0070	$MoO_4(H_2O)_{36}^{2-}$_A	1.0119	$MoS_4(H_2O)_{36}^{2-}$_A	1.0071
$MoO_4(H_2O)_{36}^{2-}$_B	1.0122	$MoS_4(H_2O)_{36}^{2-}$_B	1.0072	$MoO_4(H_2O)_{36}^{2-}$_B	1.0119	$MoS_4(H_2O)_{36}^{2-}$_B	1.0072
$MoO_4(H_2O)_{36}^{2-}$_C	1.0121	$MoS_4(H_2O)_{36}^{2-}$_C	1.0072	$MoO_4(H_2O)_{36}^{2-}$–C	1.0119	$MoS_4(H_2O)_{36}^{2-}$_C	1.0071
$MoO_4(H_2O)_{36}^{2-}$_D	1.0122	$MoS_4(H_2O)_{36}^{2-}$_D	1.0072	$MoO_4(H_2O)_{36}^{2-}$_D	1.0121	$MoS_4(H_2O)_{36}^{2-}$_D	1.0070
$MoO_4(H_2O)_{36}^{2-}$_E	1.0122	$MoS_4(H_2O)_{36}^{2-}$_E	1.0072	$MoO_4(H_2O)_{36}^{2-}$_E	1.0119	$MoS_4(H_2O)_{36}^{2-}$_E	1.0072
$MoO_4(H_2O)_{36}^{2-}$_F	1.0119	$MoS_4(H_2O)_{36}^{2-}$_F	1.0070	$MoO_4(H_2O)_{36}^{2-}$_F	1.0116	$MoS_4(H_2O)_{36}^{2-}$_F	1.0071
$MoO_4(H_2O)_{36}^{2-}$_G	1.0125	$MoS_4(H_2O)_{36}^{2-}$_G	1.0072	$MoO_4(H_2O)_{36}^{2-}$_G	1.0119	$MoS_4(H_2O)_{36}^{2-}$_G	1.0072
$MoO_4(H_2O)_{36}^{2-}$_H	1.0123	$MoS_4(H_2O)_{36}^{2-}$_H	1.0071	$MoO_4(H_2O)_{36}^{2-}$_H	1.0118	$MoS_4(H_2O)_{36}^{2-}$_H	1.0071
$MoO_4(H_2O)_{36}^{2-}$_I	1.0123	$MoS_4(H_2O)_{36}^{2-}$_I	1.0073	$MoO_4(H_2O)_{36}^{2-}$_I	1.0120	$MoS_4(H_2O)_{36}^{2-}$_I	1.0072
$MoO_4(H_2O)_{36}^{2-}$_J	1.0122	$MoS_4(H_2O)_{36}^{2-}$_J	1.0071	$MoO_4(H_2O)_{36}^{2-}$_J	1.0120	$MoS_4(H_2O)_{36}^{2-}$_J	1.0070
average	**1.0122**		**1.0072**		**1.0119**		**1.0071**
std	**0.0002**		**0.0001**		**0.0001**		**0.0001**
lnβ (‰)	**12.1**		**7.1**		**11.8**		**7.1**

[a]"Model A" denotes the ONIOM models with Mo species and the water molecules form hydrogen bonds with it as the model system. [b]"Model B" denotes the ONIOM models with only the Mo species as the model system.

Table 5. Calculated $\beta_{aq\text{-}o}$ Values for $MoO_3S(H_2O)_{36}^{2-}$, $MoO_2S_2(H_2O)_{36}^{2-}$, and $MoOS_3(H_2O)_{36}^{2-}$ at 25 °C by the ONIOM Model A

model	β	model	β	model	β
$MoO_3S(H_2O)_{36}^{2-}$_A	1.0110	$MoO_2S_2(H_2O)_{36}^{2-}$_A	1.0098	$MoOS_3(H_2O)_{36}^{2-}$_A	1.0083
$MoO_3S(H_2O)_{36}^{2-}$_B	1.0110	$MoO_2S_2(H_2O)_{36}^{2-}$_B	1.0094	$MoOS_3(H_2O)_{36}^{2-}$_B	1.0082
$MoO_3S(H_2O)_{36}^{2-}$_C	1.0112	$MoO_2S_2(H_2O)_{36}^{2-}$_C	1.0094	$MoOS_3(H_2O)_{36}^{2-}$_C	1.0083
$MoO_3S(H_2O)_{36}^{2-}$_D	1.0108	$MoO_2S_2(H_2O)_{36}^{2-}$_D	1.0095	$MoOS_3(H_2O)_{36}^{2-}$_D	1.0084
$MoO_3S(H_2O)_{36}^{2-}$_E	1.0104	$MoO_2S_2(H_2O)_{36}^{2-}$_E	1.0093	$MoOS_3(H_2O)_{36}^{2-}$_E	1.0082
$MoO_3S(H_2O)_{36}^{2-}$_F	1.0111	$MoO_2S_2(H_2O)_{36}^{2-}$_F	1.0097	$MoOS_3(H_2O)_{36}^{2-}$–F	1.0082
$MoO_3S(H_2O)_{36}^{2-}$_G	1.0109	$MoO_2S_2(H_2O)_{36}^{2-}$_G	1.0095	$MoOS_3(H_2O)_{36}^{2-}$_G	1.0085
$MoO_3S(H_2O)_{36}^{2-}$_H	1.0110	$MoO_2S_2(H_2O)_{36}^{2-}$_H	1.0095	$MoOS_3(H_2O)_{36}^{2-}$_H	1.0084
$MoO_3S(H_2O)_{36}^{2-}$–I	1.0109	$MoO_2S_2(H_2O)_{36}^{2-}$_I	1.0096	$MoOS_3(H_2O)_{36}^{2-}$_I	1.0084
$MoO_3S(H_2O)_{36}^{2-}$_J	1.0108	$MoO_2S_2(H_2O)_{36}^{2-}$_J	1.0095	$MoOS_3(H_2O)_{36}^{2-}$_J	1.0086
average	**1.0109**		**1.0095**		**1.0084**
std	**0.0002**		**0.0001**		**0.0001**
lnβ (‰)	**10.8**		**9.5**		**8.4**

0.03 Å. For $MoOS_3(H_2O)_{36}^{2-}$, d_{Mo-O} = 1.78 ± 0.01 Å and d_{Mo-S} = 2.20 ± 0.03 Å.

3.2. β Factors. *3.2.1. Isolated Molecule Results.* The calculated β values for isolated molecules with or without IEFPCM in the temperature range of 0−300 °C can be found in Tables S6 and S7. At 25 °C, $\ln\beta_{MoO_4^{2-}_{(g)}}$ = 12.4‰, $\ln\beta_{MoO_3S^{2-}_{(g)}}$ = 11.0‰, $\ln\beta_{MoO_2S_2^{2-}_{(g)}}$ = 9.7‰, $\ln\beta_{MoOS_3^{2-}_{(g)}}$ = 8.2‰, $\ln\beta_{MoS_4^{2-}_{(g)}}$ = 6.9‰, $\ln\beta_{MoO_4^{2-}_{(i)}}$ = 11.7‰, $\ln\beta_{MoO_3S^{2-}_{(i)}}$ = 10.2‰, $\ln\beta_{MoO_2S_2^{2-}_{(i)}}$ = 9.1‰, $\ln\beta_{MoOS_3^{2-}_{(i)}}$ = 7.7‰, and $\ln\beta_{MoS_4^{2-}_{(i)}}$ = 7.1‰.

3.2.2. Water-Droplet Results. The calculated $\beta_{aq\text{-}w}$ values for $MoO_4(H_2O)_n^{2-}$, $MoS_4(H_2O)_n^{2-}$, $Na_2MoO_4(H_2O)_n$, and $Na_2MoS_4(H_2O)_n$ at 25 °C by the water-droplet method are listed in Table 2. For all four systems, the β values converge as the number of water molecules increases. The calculated ln $\beta_{MoO_{4(aq\text{-}w)}^{2-}}$ = 12.2‰ and $\ln\beta_{MoS_{4(aq\text{-}w)}^{2-}}$ = 7.1‰ at 25 °C, which suggests that the co-existence of $MoO_{4(aq)}^{2-}$ and $MoS_{4(aq)}^{2-}$ results in heavy Mo enriches in $MoO_{4(aq)}^{2-}$. The Na^+ cations have little influence on the calculated $\beta_{aq\text{-}w}$ values of the Mo anions.

The calculated β values for different $MoO_4(H_2O)_{30}^{2-}$_B and $MoS_4(H_2O)_{30}^{2-}$_B models in the temperature range of 0−300 °C can be found in Table S8. At 25 °C, the explicit model produced $\ln\beta_{MoO_4^{2-}}$ = 13.0‰ and $\ln\beta_{MoS_4^{2-}}$ = 7.2‰; the explicit + D3 model produced $\ln\beta_{MoO_4^{2-}}$ = 13.11‰ and ln $\beta_{MoS_4^{2-}}$ = 7.6‰; the explicit + IEFPCM model produced ln $\beta_{MoO_4^{2-}}$ = 11.9‰ and $\ln\beta_{MoS_4^{2-}}$ = 6.9‰; the explicit + IEFPCM

https://doi.org/10.1021/acsearthspacechem.2c00268
ACS Earth Space Chem. 2023, 7, 142−155

Table 6. Polynomial Fit Parameters of the Calculated β Factors for $MoO_xS_{4-x}^{2-}$ Species in the Form of 1000 $\ln\beta = ax^3 + bx^2 + cx + d$, in Which $x = 10^6/T^2$ and T Is the Temperature in Kelvin from 273 to 573 K

species	a	b	c	d	1000 $\ln\beta$ at 25 °C
$MoO_4(H_2O)_{36}^{2-}$	0.000277	−0.020270	1.271353	0.017229	12.1
$MoO_3S(H_2O)_{36}^{2-}$	0.000329	−0.019357	1.144305	−0.042749	10.8
$MoO_2S_2(H_2O)_{36}^{2-}$	0.000230	−0.014477	0.981556	−0.061068	9.5
$MoOS_3(H_2O)_{36}^{2-}$	0.000169	−0.010431	0.841401	−0.062910	8.3
$MoS_4(H_2O)_{36}^{2-}$	0.000102	−0.006074	0.691037	−0.049573	7.1

+ D3 model produced $\ln\beta_{MoO_4^{2-}}$ = 12.2‰ and $\ln\beta_{MoS_4^{2-}}$ = 7.0‰.

3.2.3. PBC Results. The calculated $\beta_{aq\text{-}p}$ values for $Na_2MoO_4(H_2O)_{50}$ and $Na_2MoS_4(H_2O)_{50}$ at 25 °C by the PBC method are listed in Table 3. The calculated $\ln\beta_{MoO_{4(aq\text{-}p)}^{2-}}$ = 12.2‰ and $\ln\beta_{MoS_{4(aq\text{-}p)}^{2-}}$ = 7.3‰ at 25 °C, which are approximately equal to the results of the water-droplet method.

3.2.4. ONIOM Results. The calculated $\beta_{aq\text{-}o}$ values for $MoO_4(H_2O)_{36}^{2-}$ and $MoS_4(H_2O)_{36}^{2-}$ at 25 °C by the ONIOM methods are listed in Table 4. The ONIOM model A predicts $\ln\beta_{MoO_{4(aq\text{-}o)}^{2-}}$ = 12.1‰ and $\ln\beta_{MoS_{4(aq\text{-}o)}^{2-}}$ = 7.1‰ at 25 °C. The ONIOM model B predicts $\ln\beta_{MoO_{4(aq\text{-}o)}^{2-}}$ = 11.8‰ and $\ln\beta_{MoS_{4(aq\text{-}o)}^{2-}}$ = 7.1‰ at 25 °C. The standard deviations of the $\beta_{aq\text{-}o}$ values between different configurations are within ±0.0002. The ONIOM model A results agree with the results of the water-droplet and the PBC methods, while the ONIOM model B results have a slight underestimation for MoO_4^{2-}.

The calculated $\beta_{aq\text{-}o}$ values for $MoO_3S(H_2O)_{36}^{2-}$, $MoO_2S_2(H_2O)_{36}^{2-}$, and $MoOS_3(H_2O)_{36}^{2-}$ by ONIOM model A are listed in Table 5. At 25 °C, the preferred $\ln\beta_{aq\text{-}o}$ values are 10.8, 9.5, and 8.4‰ for $MoO_3S(H_2O)_{36}^{2-}$, $MoO_2S_2(H_2O)_{36}^{2-}$, and $MoOS_3(H_2O)_{36}^{2-}$, respectively.

3.3. Temperature-Dependent Equilibrium Isotope Fractionations of $MoO_xS_{4-x}^{2-}$ Species. Here, we give temperature-dependent β values of the $MoO_xS_{4-x}^{2-}$ species in the temperature range of 0−300 °C based on the results of ONIOM model A. The general equations describing the temperature-dependent β values for individual species are given in Table 6 and Figure 2. The β values show the order of $MoO_{4(aq)}^{2-}$ > $MoO_3S_{(aq)}^{2-}$ > $MoO_2S_{2(aq)}^{2-}$ > $MoOS_{3(aq)}^{2-}$ > $MoS_{4(aq)}^{2-}$, which is consistent with previous experimental results[18] and field observations.[7,11] From MoO_4^{2-} to MoS_4^{2-}, stronger Mo−O bonds are gradually substituted by weaker Mo−S bonds, and it is reasonable that the β values gradually decrease. The temperature-dependent α_{eq} values between $MoO_xS_{4-x}^{2-}$ species and MoO_4^{2-} in the aqueous phase can be found in Table S9. The calculated $\ln\alpha_{eq(MoO_xS_{4-x}^{2-}-MoO_4^{2-})}$ values at 25 °C for $MoO_3S_{(aq)}^{2-}$, $MoO_2S_{2(aq)}^{2-}$, $MoOS_{3(aq)}^{2-}$, and $MoS_{4(aq)}^{2-}$ are −1.3‰, −2.7‰, −3.8‰, and −5.0‰, respectively.

4. DISCUSSION

4.1. Evaluation of the ONIOM Method. In the definition of the ONIOM layers, the smaller size of the model system is, the fewer computational resources it needs. Thus, determining the size of the solvation shell in the model system is the key to producing β and α values accurately and efficiently. Previous formaldehyde hydration calculations showed that the solvation energy was determined mainly by the first solvation shell, and the outer-sphere solvent molecules are also necessary for long-range interactions.[79] The results of the ONIOM model A are nearly identical to the results of the water-droplet and PBC methods, but the ONIOM model B slightly overestimates the $\ln\alpha_{eq(MoS_4^{2-}-MoO_4^{2-})}$ value for 0.3‰ at 25 °C (Figure 3). Therefore, only calculating the solute molecule with a high theoretical level can introduce a small error, and the first hydration shell should be also included in the model system. The ONIOM model B results are similar to those of the IEFPCM model, which indicates that simulating all the explicit

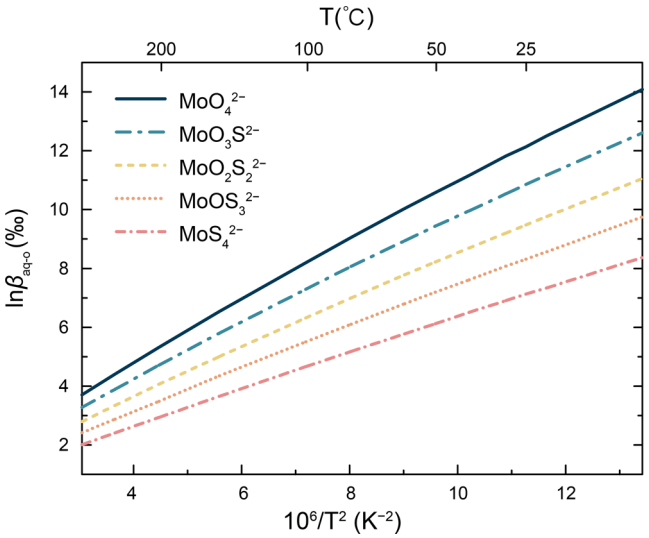

Figure 2. Calculated $\ln\beta$ (‰) values for aqueous phases at 0−300 °C by the ONIOM model A.

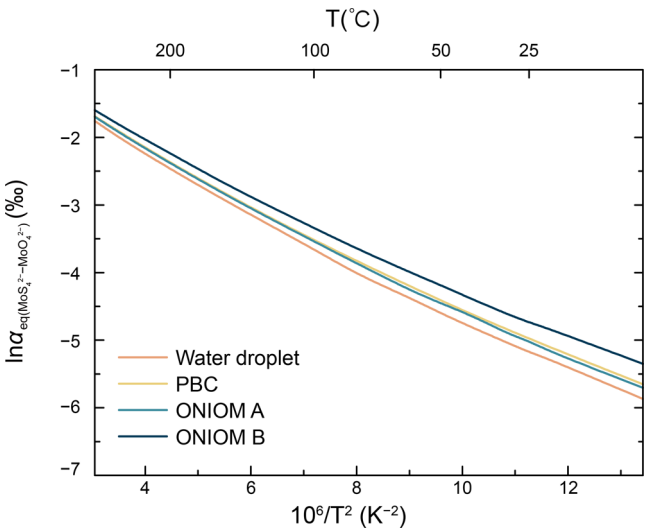

Figure 3. Comparison of the calculated $\ln\alpha_{eq(MoS_{4(aq)}^{2-}-MoO_{4(aq)}^{2-})}$ values by water-droplet, PBC, and ONIOM models at 0−300 °C.

https://doi.org/10.1021/acsearthspacechem.2c00268
ACS Earth Space Chem. 2023, 7, 142−155

water molecules at a low theoretical level is approximately the same as the IEFPCM. Considering that the standard deviation of $\ln\beta_{MoO_{4(aq)}^{2-}}$ value is 0.2‰, only treating the solute at a high level of theory is not enough for an accurate calculation of this system. For other hydrophilic and electrophilic systems, it is necessary to include water molecules directly binding to the solvent molecule in the model system to avoid large errors.

In addition, the AIMD + ONIOM method is much more convenient than the water-droplet method and is much cheaper than the FDMP + PBC method. In practice, the water-droplet method requires the researcher to manually add water molecules into a system, which may result in unreasonable initial structures that can cause convergence failure, long computational time, and unreasonable optimized structures. The procedure highly depends on the experience of the researcher. In addition, adding water molecules layer by layer and optimizing them individually is not only troublesome but also time-consuming. Based on the FPMD results, the PBC method can sample random initial structures, which is unbiased and independent of scientists' preconceptions. However, the extracted configurations from long FPMD simulations need to be relaxed for obtaining vibrational frequencies, which is expensive. The ADMP method is Car−Parrinello-type ab initio MD, which uses an extended Lagrangian to propagate the density matrix on the basis of atom-centered Gaussian functions.[72−74] The trajectory obtained by the ADMP simulation is comparable with those obtained by Born−Oppenheimer MD, and the computational costs are considerably reduced.[74] The AMDP simulation by PM6 can produce reasonable initial structures in a relatively short time for further optimization. Combining with the AMDP simulation, this work presents an efficient method that can be used to predict β values of aqueous systems with consideration of the hybrid-solvent effect.

4.2. Influences of Solvent Effects on the Predicted Equilibrium Isotope Fractionation Factors. Previous research illustrated that solvent effects can influence the predicted α_{eq} values.[27−35] The solute−solvent interactions include electrostatic forces, polarization, dispersion, repulsion, and intermolecular interactions.[80] The implicit solvent model considers the electrostatic contribution, the sum of dispersion and repulsion energies, and the energy needed to create the solute cavity in the solvent.[55] Most of the previous calculations for Mo species simulate the solvent in a homogenous constant solute cavity by the self-consistent reaction field method, that is, the implicit solvent model.[17,38−40,81]

The implicit solvent model can simulate the dielectric properties of solvents that affects the solute molecules but fails to consider the intermolecular interactions among solute and the surrounding solvent molecules. Short-distance interactions between solute and solvent molecules can largely influence the calculated α_{eq} values. For instance, the α_{eq} values of Mg between $MgHCO_{3(aq)}^{+}$ and $Mg_{(aq)}^{2+}$ with only the first shell of water molecules[82] deviated from the results with second and far coordination spheres[33] by ∼1.6‰ at 25 °C. For N and O in the NO_3^-−NO_2^-−H_2O system, the differences between the gaseous and water-droplet models are 10.2‰ for the $^{18}\beta$ values of H_2O, 1.6‰ for the $^{15}\beta$ values of NO_3^-, 5.9‰ for the $^{18}\beta$ values of NO_3^-, 6.5‰ for the $^{15}\beta$ values of NO_2^-, and 8.2‰ for the $^{18}\beta$ values of NO_2^- at 25 °C.[35] Therefore, it is necessary to incorporate explicit solvent molecules into aqueous systems. To better simulate MoO_4^{2-} in a solution system, one configuration by the implicit-plus-explicit solvent model with 12 explicit water molecules was calculated.[41] Due to the high flexibility of hydrogen bonds, the configuration of a species among water molecules is not unique.[83,84] For example, the predicted $^{30}\beta$ values of Si for SiO_4^{2-} in 32 liquid structures have a standard deviation of 0.4‰.[83] The predicted $^{18}\beta$ values of O for NO_3^- in eight liquid structures have a standard deviation of 2.3‰.[35] The significant variances emphasize the importance of solution configurational disorder. Thus, multiple configurations have to be sampled, and the β value of a species in the aqueous phase should be averaged to present the natural conditions. For the $MoO_xS_{4-x}^{2-}$ species, which are electrophobic oxyanions with a large radius, our calculation showed that increasing the number of water molecules has little influence on the β values. Therefore, the β value of MoO_4^{2-} with 12 explicit water molecules calculated in the previous study,[41] which was not provided, is expected to be comparable with our results.

Here, we present the comparison of the calculated $\ln\alpha_{eq(MoS_4^{2-}-MoO_4^{2-})}$ values by different solvent models (Figure 4). Compared with other models, the explicit model

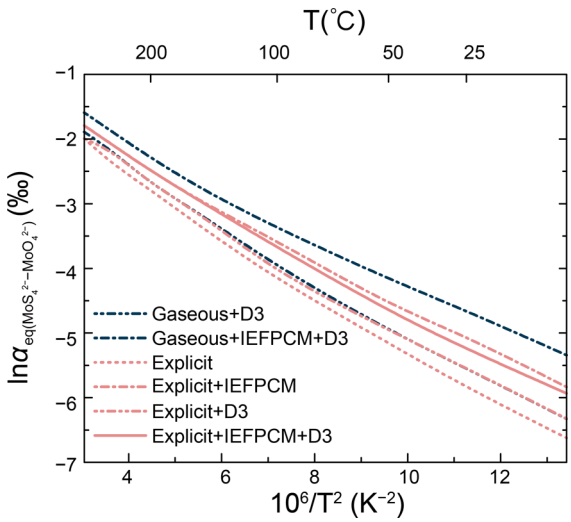

Figure 4. Comparison of the calculated $\ln\alpha_{eq(MoS_4^{2-}-MoO_4^{2-})}$ values by different solvent models at 0−300 °C.

underestimates the $\ln\alpha_{eq(MoS_4^{2-}-MoO_4^{2-})}$ values for 0.3‰ at 25 °C, while the isolated molecule with IEFPCM overestimates the $\ln\alpha_{eq(MoS_4^{2-}-MoO_4^{2-})}$ values for 0.9‰ at 25 °C. Introducing IEFPCM into the explicit model results in an increase of $\ln\alpha_{eq(MoS_4^{2-}-MoO_4^{2-})}$ values for 0.8‰ at 25 °C. The influence of the D3 dispersion correction is smaller than the IEFPCM on the explicit model, which causes $\ln\alpha_{eq(MoS_4^{2-}-MoO_4^{2-})}$ values increasing for 0.3‰ at 25 °C. The explicit + D3 model results in similar $\ln\alpha_{eq(MoS_4^{2-}-MoO_4^{2-})}$ values to the gaseous phase model. The hybrid-solvent model used in this study produces $\ln\alpha_{eq(MoS_4^{2-}-MoO_4^{2-})}$ values greater than the explicit + D3 model for 0.3‰ at 25 °C but smaller than the explicit + IEFPCM model for 0.2‰ at 25 °C. The results suggest that it is necessary to include an implicit solvent model, explicit solvent molecules, and dispersion correction when calculating the α_{eq} values for species in the aqueous phase.

4.3. Isotope Fractionation Factors between $MoO_xS_{4-x}^{2-}$ Species. Considering IEFPCM, the previously

https://doi.org/10.1021/acsearthspacechem.2c00268
ACS Earth Space Chem. 2023, 7, 142−155

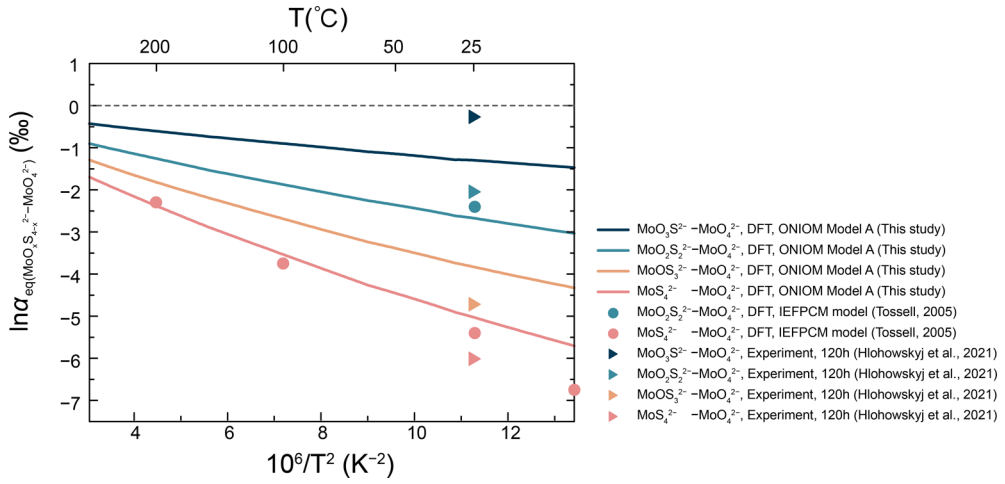

Figure 5. Comparison of calculated lnα_{eq} values between $MoO_xS_{4-x}^{2-}$ and MoO_4^{2-} at 0−300 °C with the literature.

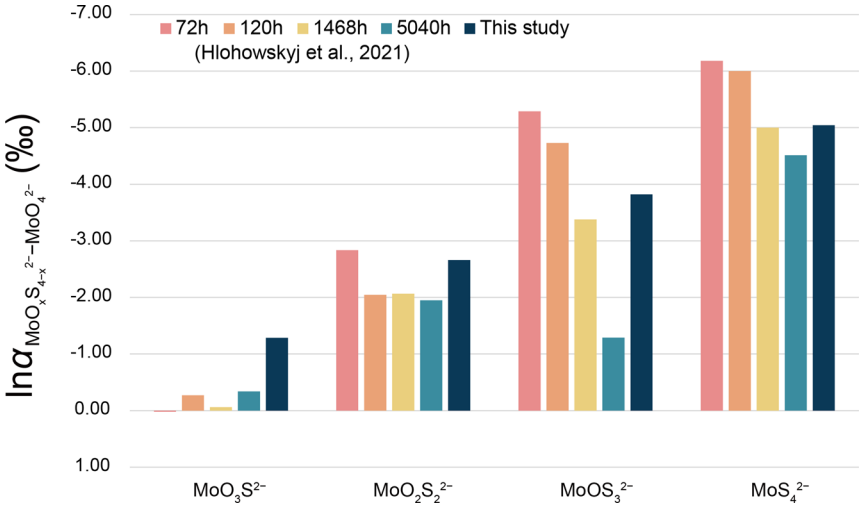

Figure 6. Comparison of ln $\alpha_{MoO_xS_{4-x}^{2-}-MoO_4^{2-}}$ between calculation at 25 °C with laboratory experiments at room temperature for 72−5040 h.[18]

calculated ln$\alpha_{MoO_2S_2^{2-}-MoO_4^{2-}}$ and ln$\alpha_{MoS_{4(g)}^{2-}-MoO_{4(g)}^{2-}}$ values at 25 °C are −5.4‰ and −2.4‰ by the B3LYP method, respectively, and −6.8‰ and −3.3‰ by the HF method, respectively.[17] The small discrepancies between the previous work and this work may be related to the fact that the previous study did not consider the explicit water molecules (Figure 5).

Based on the thiolation experiments, the temporal α factors between $MoO_xS_{4-x}^{2-}$ species and MoO_4^{2-} have been reported.[18] Compared to the previous calculation results,[17] the α values among $MoO_xS_{4-x}^{2-}$ species are considered under *relative "equilibrium" conditions* at 120 h of equilibration.[18] Under this condition, the determined ln $\alpha_{MoO_2S_2^{2-}-MoO_4^{2-}}$ = −3.76‰ is close to the results of the HF method, while the determined ln $\alpha_{MoS_4^{2-}-MoO_4^{2-}}$ = −5.51‰ is close to the results of the B3LYP method.[17,18] Figure 6 illustrates the α factors in the experiments from 72 h to 7 months[17] and compares them with our calculated α_{eq} factors. Both the experimental and theoretical results indicate that the α values between $MoO_xS_{4-x}^{2-}$ and MoO_4^{2-} are positively related to the number of S atoms in the solute molecules. The experimental results at 120 h are roughly in line with our calculation results. However, for a longer experimental period, species concentrations and isotope compositions kept changing for all Mo species, especially that the $\delta^{98}Mo_{MoOS_3^{2-}}$ value changed from −0.73‰ at 3 months to +0.70‰ at 7 months.[18] It is hard to tell whether the equilibrium had been reached or had been disrupted after 120 h. Nevertheless, our calculated α_{eq} factors are close to the experimental results at 3 months except for MoO_3S^{2-}.

5. IMPLICATIONS

5.1. Mo Isotopes as a Paleoredox Proxy. In well-oxygenated settings, MoO_4^{2-} is the dominant species. About 30−50% MoO_4^{2-} coprecipitates with (Fe, Mn)-oxyhydroxides,[12] with an isotope fractionation up to −3‰.[8,40] The observed δ^{98}Mo value in oxyhydroxides varies in a narrow range between −1.0‰ and −0.5‰.[85] In strongly euxinic settings, thiomolybdate sequestration occurs efficiently by adsorption on organic matter and/or precipitation as authigenic sulfide minerals[10,11,86−90] with a rate 2 to 3 orders faster than that in oxic environments.[91,92] The precipitation of thiomolybdates in strongly euxinic settings produces a small isotope fractionation of −0.3‰ to 0‰ between seawater and sediments.[7,93] Since the thiomolybdates precipitate rapidly and completely in the strongly euxinic sediments from restricted marine basins, such as the deep Black Sea (below ∼1000 m), the δ^{98}Mo value of the sediments has been used to represent

https://doi.org/10.1021/acsearthspacechem.2c00268
ACS Earth Space Chem. 2023, 7, 142−155

the global seawater δ^{98}Mo value.[6,7,23] The observed δ^{98}Mo value of strongly euxinic sediments also varies in a narrow range between 1.7‰ and 2.4‰.[7,24] Nevertheless, a nontrivial isotope fractionation factor of −0.5 ± 0.3‰ for MoS_4^{2-} or $MoOS_3^{2-}$ precipitation was expected,[22] which needs to be further tested.

The processes in well-oxygenated and strongly euxinic settings have been well studied, but in suboxic, ferruginous, and weakly euxinic settings, the mechanisms and the associated isotope fractionation factors remain unclear.[12,14] It has been observed that the δ^{98}Mo values in weakly euxinic sediments vary in a wide range from −0.6‰ to 1.8‰, which are in between those of well-oxygenated and strongly euxinic sediments.[7,24] Such a variation has been explained by the incomplete conversion of molybdate to thiomolybdates.[1,2,7,21−23,85] According to our predictions, the δ^{98}Mo values of mono-, di-, tri-, and tetra-thiomolybdates in seawater vary for 3.7‰ under the equilibrium condition. Such a variation can explain the observed δ^{98}Mo value variation in weakly euxinic sediments. Thus, it is reasonable to propose that the removal of Mo in weakly euxinic settings is a combination of molybdate and thiomolybdate precipitation.

The competition between thiolation and precipitation causes problems in the quantitative interpretation of the δ^{98}Mo values in sediments. This hampers the quantitative reconstruction of marine Mo cycling and oceanic oxygenation extent throughout the Earth's history. Using Mo isotopes as a paleoredox proxy requires constraints on the reaction rates among the $MoO_xS_{4-x}^{2-}$ species, the precipitation rates of each species, and the isotope fractionation factors for all the processes. The precipitation of $MoO_xS_{4-x}^{2-}$ species is not fully understood. Further studies are necessary to reveal the Mo isotope fractionations during the precipitation of the thiomolybdates. Even so, our results could shed light upon the Mo isotope behaviors in suboxic, ferruginous, and weakly euxinic settings.

5.2. ONIOM Method for Mo Species Adsorption on Water-Mineral Surfaces. Besides the speciation transformation, the isotope fractionation caused by precipitation also controls the δ^{98}Mo values recorded in sediments. The experimentally observed α values for MoO_4^{2-} precipitation on (Fe, Mn)-oxyhydroxides are about −2‰ to −3‰.[12] Previous DFT calculations discussed possible adsorption mechanisms. At 25 °C, the $\ln\alpha_{eq}$ value between MoO_3 and MoO_4^{2-} is −2.4‰, which suggested that, in oxic ocean water, Mo transforms from a four-coordinate MoO_4^{2-} to a three-coordinate MoO_3 on the surface of (Fe, Mn)-oxyhydroxides.[17] Comparing Raman spectroscopy results of solution with the DFT calculation results of gaseous phase molecules, the adsorption structure of MoO_4^{2-} on the (Fe, Mn)-oxyhydroxide surface was proposed to be $MoO_3(H_2O)_3$.[81] However, the calculated $\ln\alpha_{eq}$ values between $MoO_3(H_2O)_3$ and MoO_4^{2-} (−0.57‰) could not explain the observed large α values.[38,39] Based on X-ray absorption fine structure results and DFT calculation, the adsorption of MoO_4^{2-} on a permissive surface was proposed to be polynuclear in distorted octahedral coordination with oxygen.[40] The calculated $\ln\alpha_{eq}$ values of hexamolybdate ($Mo_6O_{19}^{2-}$) and MoO_4^{2-} are consistent with the experimental fractionation factors under 1−50 °C.[94]

The above-mentioned works calculated the β values of isolated molecules or a $Mo_6O_{19}^{2-}$ cluster, which cannot be direct evidence for the surface adsorption mechanism in solution. Using the DFT method, the adsorption structures of nondistorted octahedral, distorted octahedral, and dimeric forms on manganese oxide (MnO_2) sheets were calculated by cluster models.[41] The calculated $\ln\alpha_{eq}$ values between MnO_2-adsorbed Mo species and MoO_4^{2-} in the aqueous phase are in the range of −2.43‰ to −3.30‰,[41] which are consistent with previous calculations[40] and precipitation experiments.[94] Such adsorption models used a cluster with two Mn atoms and three explicit water molecules, and the whole system included about 30 atoms. Using the ab initio MD method, the adsorption geometry and energy of MoO_4^{2-} on gothite were calculated with consideration of explicit water molecules.[95] This model used a cluster model with one layer of goethite with 16 Fe atoms, and the whole system included almost 200 atoms. The calculation of vibrational frequencies for such a system is too expensive. Therefore, based on the surface complexation model, it was estimated that the $\ln\alpha_{eq}$ values between gothite-adsorbed Mo species and MoO_4^{2-} in the aqueous phase should be in the range of −1.6‰ to −2.3‰.[95]

The limitation of surface adsorption equilibrium isotope fractionation calculation is mainly due to the restriction of computation resources. Except for the explicit solvent model, the ONIOM method has also been used for surface calculation.[96−98] Using the ONIOM method, we should be able to construct a larger mineral surface cluster with explicit solvent molecules to represent the water-mineral surface. The massive computational resources required for vibrational frequencies should be reduced by treating the adsorption center with a higher theoretical level and the outer parts with a lower theoretical level. Therefore, the ONIOM method has the potential to be used in equilibrium isotope fractionation calculation for the water-mineral surface process, which needs to be further explored.

6. CONCLUSIONS

The existence of water fundamentally altered the state of our planet. Chemical reactions in the aqueous phase play a key role in the element cycles on the Earth's surface. Isotope effects, which can be predicted accurately and efficiently by QMs, characterize a defined process and therefore can be used to deduce reaction mechanisms in complex reaction systems. In this work, we systematically test different methods to calculate equilibrium isotope fractionation factors among $MoO_xS_{4-x}^{2-}$ species in the aqueous phase by a hybrid-solvent model. The results show that the ONIOM method can accurately predict the β values with a considerable reduction of computational resources, which can be used as references for experiments and field observations. This work finds that there are significantly lighter Mo isotope enrichments occurring during the thiolation of molybdate. It is necessary to consider the isotope fractionation among $MoO_xS_{4-x}^{2-}$ species when using Mo isotope paleoredox proxy, especially in suboxic, ferruginous, and weakly euxinic settings.

■ ASSOCIATED CONTENT

Supporting Information

The Supporting Information is available free of charge at https://pubs.acs.org/doi/10.1021/acsearthspacechem.2c00268.

Selected geometric parameters, β values for isolated molecules, data for Figures 2, 4, and 5, all the optimized structure coordinates, and a script used to prepare the water cluster structures with given numbers of water molecules (PDF)

https://doi.org/10.1021/acsearthspacechem.2c00268
ACS Earth Space Chem. 2023, 7, 142−155

β values calculated for all the monomers, ONIOM, water-droplet models, and PBC models (XLSX)

AUTHOR INFORMATION

Corresponding Author

Yuyang He − *Key Laboratory of Earth and Planetary Physics, Institute of Geology and Geophysics, Chinese Academy of Sciences, Beijing 100029, China; State Key Laboratory of High Temperature Gas Dynamics, Institute of Mechanics, Chinese Academy of Sciences, Beijing 100190, China;* orcid.org/0000-0003-3220-1432; Email: yhe@mail.iggcas.ac.cn

Authors

Caihong Gao − *State Key Laboratory of Ore Deposit Geochemistry, Institute of Geochemistry, Chinese Academy of Sciences, Guiyang, Guizhou 550081, China*

Wei Wei − *CAS Key Laboratory of Crust-Mantle Materials and Environments, School of Earth and Space Sciences, University of Science and Technology of China, Hefei, Anhui 230026, China;* orcid.org/0000-0002-9729-4345

Yun Liu − *State Key Laboratory of Ore Deposit Geochemistry, Institute of Geochemistry, Chinese Academy of Sciences, Guiyang, Guizhou 550081, China; International Center for Planetary Science, College of Earth Sciences, Chengdu University of Technology, Chengdu, Sichuan 610059, China;* orcid.org/0000-0003-1000-143X

Complete contact information is available at: https://pubs.acs.org/10.1021/acsearthspacechem.2c00268

Author Contributions

#Y.H. and C.G. have contributed equally.

Notes

The authors declare no competing financial interest.

ACKNOWLEDGMENTS

The authors are grateful for the valuable discussions with Xiaosong Li, Junzhi Ding, and Yining Zhang. This study was supported by the National Science Foundation of China (NSFC) projects 4217030170 and 42150202 and the preresearch project on Civil Aerospace Technologies of China National Space Administration (D020203) to Y.H., the NSFC project (41903019 and 42130114) and the strategic priority research program (B) of CAS (XDB41000000) to C.G. and Y. L., and the NSFC project (41902025) to W.W.

REFERENCES

(1) Arnold, G. L.; Anbar, A. D.; Barling, J.; Lyons, T. W. Molybdenum Isotope Evidence for Widespread Anoxia in Mid-Proterozoic Oceans. *Science* **2004**, *304*, 87−90.

(2) Dahl, T. W.; Anbar, A. D.; Gordon, G. W.; Rosing, M. T.; Frei, R.; Canfield, D. E. The Behavior of Molybdenum and Its Isotopes across the Chemocline and in the Sediments of Sulfidic Lake Cadagno, Switzerland. *Geochim. Cosmochim. Acta* **2010**, *74*, 144−163.

(3) Chen, X.; Ling, H.-F.; Vance, D.; Shields-Zhou, G. A.; Zhu, M.; Poulton, S. W.; Och, L. M.; Jiang, S.-Y.; Li, D.; Cremonese, L.; Archer, C. Rise to Modern Levels of Ocean Oxygenation Coincided with the Cambrian Radiation of Animals. *Nat. Commun.* **2015**, *6*, 7142.

(4) Dickson, A. J. A. Molybdenum-Isotope Perspective on Phanerozoic Deoxygenation Events. *Nat. Geosci.* **2017**, *10*, 721−726.

(5) Wei, G.-Y.; Planavsky, N. J.; He, T.; Zhang, F.; Stockey, R. G.; Cole, D. B.; Lin, Y.-B.; Ling, H.-F. Global Marine Redox Evolution from the Late Neoproterozoic to the Early Paleozoic Constrained by the Integration of Mo and U Isotope Records. *Earth-Sci. Rev.* **2021**, *214*, 103506.

(6) Barling, J.; Arnold, G. L.; Anbar, A. D. Natural Mass-Dependent Variations in the Isotopic Composition of Molybdenum. *Earth Planet. Sci. Lett.* **2001**, *193*, 447−457.

(7) Neubert, N.; Nägler, T. F.; Böttcher, M. E. Sulfidity Controls Molybdenum Isotope Fractionation into Euxinic Sediments: Evidence from the Modern Black Sea. *Geology* **2008**, *36*, 775−778.

(8) Brucker, R. L. P.; McManus, J.; Severmann, S.; Berelson, W. M. Molybdenum Behavior during Early Diagenesis: Insights from Mo Isotopes. *Geochem., Geophys., Geosyst.* **2009**, *10* (6), 1−25.

(9) Kendall, B.; Wang, J.; Zheng, W.; Romaniello, S. J.; Over, D. J.; Bennett, Y.; Xing, L.; Kunert, A.; Boyes, C.; Liu, J. Inverse Correlation between the Molybdenum and Uranium Isotope Compositions of Upper Devonian Black Shales Caused by Changes in Local Depositional Conditions Rather than Global Ocean Redox Variations. *Geochim. Cosmochim. Acta* **2020**, *287*, 141−164.

(10) Helz, G. R.; Miller, C. V.; Charnock, J. M.; Mosselmans, J. F. W.; Pattrick, R. A. D.; Garner, C. D.; Vaughan, D. J. Mechanism of Molybdenum Removal from the Sea and Its Concentration in Black Shales: EXAFS Evidence. *Geochim. Cosmochim. Acta* **1996**, *60*, 3631−3642.

(11) Erickson, B. E.; Helz, G. R. Molybdenum (VI) Speciation in Sulfidic Waters:: Stability and Lability of Thiomolybdates. *Geochim. Cosmochim. Acta* **2000**, *64*, 1149−1158.

(12) Kendall, B.; Dahl, T. W.; Anbar, A. D. The Stable Isotope Geochemistry of Molybdenum. *Rev. Mineral. Geochem.* **2017**, *82*, 683−732.

(13) Smedley, P. L.; Kinniburgh, D. G. Molybdenum in Natural Waters: A Review of Occurrence, Distributions and Controls. *Appl. Geochem.* **2017**, *84*, 387−432.

(14) Phillips, R.; Xu, J. A Critical Review of Molybdenum Sequestration Mechanisms under Euxinic Conditions: Implications for the Precision of Molybdenum Paleoredox Proxies. *Earth-Sci. Rev.* **2021**, *221*, 103799.

(15) Chen, G.; Ford, T. E.; Clayton, C. R. Interaction of Sulfate-Reducing Bacteria with Molybdenum Dissolved from Sputter-Deposited Molybdenum Thin Films and Pure Molybdenum Powder. *J. Colloid Interface Sci.* **1998**, *204*, 237−246.

(16) Deng, X.; Dohmae, N.; Kaksonen, A. H.; Okamoto, A. Biogenic Iron Sulfide Nanoparticles to Enable Extracellular Electron Uptake in Sulfate-Reducing Bacteria. *Angew. Chem., Int. Ed.* **2020**, *132*, 5906.

(17) Tossell, J. A. Calculating the Partitioning of the Isotopes of Mo between Oxidic and Sulfidic Species in Aqueous Solution. *Geochim. Cosmochim. Acta* **2005**, *69*, 2981−2993.

(18) Hlohowskyj, S. R.; Chen, X.; Romaniello, S. J.; Vorlicek, T. P.; Anbar, A. D.; Lyons, T. W.; Chappaz, A. Quantifying Molybdenum Isotopic Speciation in Sulfidic Water: Implications for the Paleoredox Proxy. *ACS Earth Space Chem.* **2021**, *5*, 2891−2899.

(19) Scott, C.; Lyons, T. W. Contrasting Molybdenum Cycling and Isotopic Properties in Euxinic versus Non-Euxinic Sediments and Sedimentary Rocks: Refining the Paleoproxies. *Chem. Geol.* **2012**, *324*−*325*, 19−27.

(20) Poulson, R. L.; Siebert, C.; McManus, J.; Berelson, W. M. Authigenic Molybdenum Isotope Signatures in Marine Sediments. *Geology* **2006**, *34*, 617−620.

(21) Dahl, T. W.; Hammarlund, E. U.; Anbar, A. D.; Bond, D. P. G.; Gill, B. C.; Gordon, G. W.; Knoll, A. H.; Nielsen, A. T.; Schovsbo, N. H.; Canfield, D. E. Devonian Rise in Atmospheric Oxygen Correlated to the Radiations of Terrestrial Plants and Large Predatory Fish. *Proc. Natl. Acad. Sci. U.S.A.* **2010**, *107*, 17911−17915.

(22) Nägler, T. F.; Neubert, N.; Böttcher, M. E.; Dellwig, O.; Schnetger, B. Molybdenum Isotope Fractionation in Pelagic Euxinia: Evidence from the Modern Black and Baltic Seas. *Chem. Geol.* **2011**, *289*, 1−11.

(23) Noordmann, J.; Weyer, S.; Montoya-Pino, C.; Dellwig, O.; Neubert, N.; Eckert, S.; Paetzel, M.; Böttcher, M. E. Uranium and Molybdenum Isotope Systematics in Modern Euxinic Basins: Case

Studies from the Central Baltic Sea and the Kyllaren Fjord (Norway). *Chem. Geol.* **2015**, *396*, 182−195.
(24) Zhang, Y.; Wen, H.; Zhu, C.; Fan, H.; Xiao, J.; Wen, J. Molybdenum Isotopic Evidence for Anoxic Marine Conditions during the End-Permian Mass Extinction. *Chem. Geol.* **2021**, *575*, 120259.
(25) Urey, H. C. The Thermodynamic Properties of Isotopic Substances. *J. Chem. Soc.* **1947**, 562−581.
(26) Bigeleisen, J.; Mayer, M. Calculation of Equilibrium Constants for Isotopic Exchange Reactions. *J. Chem. Phys.* **1947**, *15*, 261−267.
(27) Liu, Y.; Tossell, J. A. Ab Initio Molecular Orbital Calculations for Boron Isotope Fractionations on Boric Acids and Borates. *Geochim. Cosmochim. Acta* **2005**, *69*, 3995−4006.
(28) Rustad, J. R.; Nelmes, S. L.; Jackson, V. E.; Dixon, D. A. Quantum-Chemical Calculations of Carbon-Isotope Fractionation in $CO_{2(g)}$, Aqueous Carbonate Species, and Carbonate Minerals. *J. Phys. Chem. A* **2008**, *112*, 542−555.
(29) Rustad, J. R.; Casey, W. H.; Yin, Q.-Z.; Bylaska, E. J.; Felmy, A. R.; Bogatko, S. A.; Jackson, V. E.; Dixon, D. A. Isotopic Fractionation of $Mg^{2+}_{(Aq)}$, $Ca^{2+}_{(Aq)}$, and $Fe^{2+}_{(Aq)}$ with Carbonate Minerals. *Geochim. Cosmochim. Acta* **2010**, *74*, 6301−6323.
(30) Zhang, S.; Liu, Y. Molecular-Level Mechanisms of Quartz Dissolution under Neutral and Alkaline Conditions in the Presence of Electrolytes. *Geochem. J.* **2014**, *48*, 189−205.
(31) He, H.; Liu, Y. Silicon Isotope Fractionation during the Precipitation of Quartz and the Adsorption of $H_4SiO_{4(Aq)}$ on Fe(III)-Oxyhydroxide Surfaces. *Chin. J. Geochem.* **2015**, *34*, 459−468.
(32) Zeebe, R. E. Oxygen Isotope Fractionation between Water and the Aqueous Hydroxide Ion. *Geochim. Cosmochim. Acta* **2020**, *289*, 182−195.
(33) Gao, C.; Cao, X.; Liu, Q.; Yang, Y.; Zhang, S.; He, Y.; Tang, M.; Liu, Y. Theoretical Calculation of Equilibrium Mg Isotope Fractionations between Minerals and Aqueous Solutions. *Chem. Geol.* **2018**, *488*, 62−75.
(34) Li, L.; He, Y.; Zhang, Z.; Liu, Y. Nitrogen Isotope Fractionations among Gaseous and Aqueous NH_4^+, NH_3, N_2, and Metal-Ammine Complexes: Theoretical Calculations and Applications. *Geochim. Cosmochim. Acta* **2021**, *295*, 80−97.
(35) He, Y.; Li, L. Density Functional Theory Calculations of Nitrogen and Oxygen Equilibrium Isotope Fractionations in NO_3^-−NO_2^-−H_2O Aqueous System Reveal Inverse Kinetic Isotope Effects during Nitrite Oxidation. *Appl. Geochem.* **2022**, *139*, 105265.
(36) Chung, L. W.; Sameera, W. M. C.; Ramozzi, R.; Page, A. J.; Hatanaka, M.; Petrova, G. P.; Harris, T. V.; Li, X.; Ke, Z.; Liu, F.; Li, H.-B.; Ding, L.; Morokuma, K. The ONIOM Method and Its Applications. *Chem. Rev.* **2015**, *115*, 5678−5796.
(37) Anbar, A. D.; Duan, Y.; Lyons, T. W.; Arnold, G. L.; Kendall, B.; Creaser, R. A.; Kaufman, A. J.; Gordon, G. W.; Scott, C.; Garvin, J.; Buick, R. A Whiff of Oxygen before the Great Oxidation Event? *Science* **2007**, *317*, 1903−1906.
(38) Weeks, C. L.; Anbar, A. D.; Wasylenki, L. E.; Spiro, T. G. Density Functional Theory Analysis of Molybdenum Isotope Fractionation. *J. Phys. Chem. A* **2007**, *111*, 12434−12438.
(39) Weeks, C. L.; Anbar, A. D.; Wasylenki, L. E.; Spiro, T. G. Density Functional Theory Analysis of Molybdenum Isotope Fractionation. *J. Phys. Chem. A* **2008**, *112*, 10703−10704.
(40) Wasylenki, L. E.; Weeks, C. L.; Bargar, J. R.; Spiro, T. G.; Hein, J. R.; Anbar, A. D. The Molecular Mechanism of Mo Isotope Fractionation during Adsorption to Birnessite. *Geochim. Cosmochim. Acta* **2011**, *75*, 5019−5031.
(41) Tanaka, M.; Ariga, D.; Kashiwabara, T.; Takahashi, Y. Adsorption Mechanism of Molybdenum (VI) on Manganese Oxides Causing a Large Isotope Fractionation. *ACS Earth Space Chem.* **2018**, *2*, 1187−1195.
(42) Siebert, C.; Nägler, T. F.; Kramers, J. D. Determination of Molybdenum Isotope Fractionation by Double-Spike Multicollector Inductively Coupled Plasma Mass Spectrometry. *Geochem., Geophys., Geosyst.* **2001**, *2*, No. 2000GC000124.
(43) Neely, R. A.; Gislason, S. R.; Ólafsson, M.; McCoy-West, A. J.; Pearce, C. R.; Burton, K. W. Molybdenum Isotope Behaviour in Groundwaters and Terrestrial Hydrothermal Systems, Iceland. *Earth Planet. Sci. Lett.* **2018**, *486*, 108−118.
(44) Ostrander, C. M.; Sahoo, S. K.; Kendall, B.; Jiang, G.; Planavsky, N. J.; Lyons, T. W.; Nielsen, S. G.; Owens, J. D.; Gordon, G. W.; Romaniello, S. J.; Anbar, A. D. Multiple Negative Molybdenum Isotope Excursions in the Doushantuo Formation (South China) Fingerprint Complex Redox-Related Processes in the Ediacaran Nanhua Basin. *Geochim. Cosmochim. Acta* **2019**, *261*, 191−209.
(45) Zhu, H.-G.; Zhu, J.-M.; Tan, D.; Lin, X.; Lu, K.; Yang, W. Validating the High-Precision Measurement of Mo Isotopes at the 5 Ng Level Using Double Spike MC-ICP-MS. *J. Anal. At. Spectrom.* **2022**, *37*, 1063−1075.
(46) Richet, P.; Bottinga, Y.; Javoy, M. A Review of Hydrogen, Carbon, Nitrogen, Oxygen, Sulphur, and Chlorine Stable Isotope Enrichment among Gaseous Molecules. *Annu. Rev. Earth Planet. Sci.* **1977**, *5*, 65−110.
(47) Schauble, E. A. Applying Stable Isotope Fractionation Theory to New Systems. *Rev. Mineral. Geochem.* **2004**, *55*, 65−111.
(48) Cao, X.; Liu, Y. Theoretical Estimation of the Equilibrium Distribution of Clumped Isotopes in Nature. *Geochim. Cosmochim. Acta* **2012**, *77*, 292−303.
(49) Liu, Q.; Tossell, J. A.; Liu, Y. On the Proper Use of the Bigeleisen−Mayer Equation and Corrections to It in the Calculation of Isotopic Fractionation Equilibrium Constants. *Geochim. Cosmochim. Acta* **2010**, *74*, 6965−6983.
(50) Méheut, M.; Lazzeri, M.; Balan, E.; Mauri, F. Equilibrium Isotopic Fractionation in the Kaolinite, Quartz, Water System: Prediction from First-Principles Density-Functional Theory. *Geochim. Cosmochim. Acta* **2007**, *71*, 3170−3181.
(51) Schauble, E. A.; Ghosh, P.; Eiler, J. M. Preferential Formation of 13C−18O Bonds in Carbonate Minerals, Estimated Using First-Principles Lattice Dynamics. *Geochim. Cosmochim. Acta* **2006**, *70*, 2510−2529.
(52) He, Y.; Zhang, Y.; Zhang, S.; Liu, Y. Predicting Nitrogen and Oxygen Kinetic Isotope Effects of Nitrate Reduction by Periplasmic Dissimilatory Nitrate Reductase. *Geochim. Cosmochim. Acta* **2021**, *293*, 224−239.
(53) Frisch, M. J.; Trucks, G. W.; Schlegel, H. B.; Scuseria, G. E.; Robb, M. A.; Cheeseman, J. R.; Scalmani, G.; Barone, V.; Petersson, G. A.; Nakatsuji, H.; Li, X.; Caricato, M.; Marenich, A. V.; Bloino, J.; Janesko, B. G.; Gomperts, R.; Mennucci, B.; Hratchian, H. P.; Ortiz, J. V.; Izmaylov, A. F.; Sonnenberg, J. L.; Williams-Young, D.; Ding, F.; Lipparini, F.; Egidi, F.; Goings, J.; Peng, B.; Petrone, A.; Henderson, T.; Ranasinghe, D.; Zakrzewski, V. G.; Gao, J.; Rega, N.; Zheng, G.; Liang, W.; Hada, M.; Ehara, M.; Toyota, K.; Fukuda, R.; Hasegawa, J.; Ishida, M.; Nakajima, T.; Honda, Y.; Kitao, O.; Nakai, H.; Vreven, T.; Throssell, K.; Montgomery, J. A., Jr.; Peralta, J. E.; Ogliaro, F.; Bearpark, M. J.; Heyd, J. J.; Brothers, E. N.; Kudin, K. N.; Staroverov, V. N.; Keith, T. A.; Kobayashi, R.; Normand, J.; Raghavachari, K.; Rendell, A. P.; Burant, J. C.; Iyengar, S. S.; Tomasi, J.; Cossi, M.; Millam, J. M.; Klene, M.; Adamo, C.; Cammi, R.; Ochterski, J. W.; Martin, R. L.; Morokuma, K.; Farkas, O.; Foresman, J. B.; Fox, D. J.*Gaussian 16*, Revision C.01; Gaussian, Inc., 2019.
(54) Kresse, G.; Furthmüller, J. Efficient Iterative Schemes for Ab Initio Total-Energy Calculations Using a Plane-Wave Basis Set. *Phys. Rev. B: Condens. Matter Mater. Phys.* **1996**, *54*, 11169−11186.
(55) Scalmani, G.; Frisch, M. J. Continuous Surface Charge Polarizable Continuum Models of Solvation. I. General Formalism. *J. Chem. Phys.* **2010**, *132*, 114110.
(56) Lee, C.; Yang, W.; Parr, R. G. Development of the Colle-Salvetti Correlation-Energy Formula into a Functional of the Electron Density. *Phys. Rev. B: Condens. Matter Mater. Phys.* **1988**, *37*, 785.
(57) Becke, A. D. Density-Functional Thermochemistry. III. The Role of Exact Exchange. *J. Chem. Phys.* **1993**, *98*, 5648.
(58) Hay, P. J.; Wadt, W. R. Ab Initio Effective Core Potentials for Molecular Calculations. Potentials for K to Au Including the Outermost Core Orbitals. *J. Chem. Phys.* **1985**, *82*, 299−310.

(59) Wadt, W. R.; Hay, P. J. Ab Initio Effective Core Potentials for Molecular Calculations. Potentials for Main Group Elements Na to Bi. *J. Chem. Phys.* **1985**, *82*, 284−298.
(60) Krishnan, R.; Binkley, J. S.; Seeger, R.; Pople, J. A. Self-Consistent Molecular Orbital Methods. XX. A Basis Set for Correlated Wave Functions. *J. Chem. Phys.* **1980**, *72*, 650−654.
(61) McLean, A. D.; Chandler, G. S. Contracted Gaussian Basis Sets for Molecular Calculations. I. Second Row Atoms, Z = 11−18. *J. Chem. Phys.* **1980**, *72*, 5639−5648.
(62) Grimme, S.; Antony, J.; Ehrlich, S.; Krieg, H. A Consistent and Accurate Ab Initio Parametrization of Density Functional Dispersion Correction (DFT-D) for the 94 Elements H-Pu. *J. Chem. Phys.* **2010**, *132*, 154104.
(63) Grimme, S. Density Functional Theory with London Dispersion Corrections. *Wiley Interdiscip. Rev. Comput. Mol. Sci.* **2011**, *1*, 211−228.
(64) Perdew, J. P.; Burke, K.; Ernzerhof, M. Generalized Gradient Approximation Made Simple. *Phys. Rev. Lett.* **1996**, *77*, 3865−3868.
(65) Parlinski, K.; Li, Z. Q.; Kawazoe, Y. First-Principles Determination of the Soft Mode in Cubic ZrO_2. *Phys. Rev. Lett.* **1997**, *78*, 4063−4066.
(66) Chung, L. W.; Hirao, H.; Li, X.; Morokuma, K. The ONIOM Method: Its Foundation and Applications to Metalloenzymes and Photobiology. *Wiley Interdiscip. Rev. Comput. Mol. Sci.* **2012**, *2*, 327−350.
(67) Re, S.; Morokuma, K. ONIOM Study of Chemical Reactions in Microsolvation Clusters: $(H_2O)_nCH_3Cl$+ OH-$(H_2O)_m$ (N+ M= 1 and 2). *J. Phys. Chem. A* **2001**, *105*, 7185−7197.
(68) Re, S.; Morokuma, K. Own N-Layered Integrated Molecular Orbital and Molecular Mechanics Study of the Reaction of OH- with Polychlorinated Hydrocarbons $CH_{(4-n)}Cl_n$ (N= 2−4). *Theor. Chem. Acc.* **2004**, *112*, 59−67.
(69) Fukaya, H.; Morokuma, K. A. Theoretical Study of the Mechanism of Selective Fluorination of Saturated Hydrocarbons by Molecular Fluorine. Participation of $CHCl_3$ Solvent Molecules in the Ionic Process. *J. Org. Chem.* **2003**, *68*, 8170−8178.
(70) Maeda, S.; Ohno, K.; Morokuma, K. An Automated and Systematic Transition Structure Explorer in Large Flexible Molecular Systems Based on Combined Global Reaction Route Mapping and Microiteration Methods. *J. Chem. Theory Comput.* **2009**, *5*, 2734−2743.
(71) Ando, K.; Morokuma, K. DFT and ONIOM Study on the Alkylation of the Lithium Enolate in Solution: Microsolvation Cluster Models for CH_2=CHOLi + CH_3Cl+$(THF)_{0-6}$. *Theor. Chem. Acc.* **2011**, *130*, 323−331.
(72) Iyengar, S. S.; Schlegel, H. B.; Millam, J. M.; Voth, G. A.; Scuseria, E. G.; Frisch, M. J. Ab Initio Molecular Dynamics: Propagating the Density Matrix with Gaussian Orbitals. II. Generalizations Based on Mass-Weighting, Idempotency, Energy Conservation and Choice of Initial Conditions. *J. Chem. Phys.* **2001**, *115*, 10291−10302.
(73) Schlegel, H. B.; Millam, J. M.; Iyengar, S. S.; Voth, G. A.; Daniels, A. D.; Scuseria, G. E.; Frisch, M. J. Ab Initio Molecular Dynamics: Propagating the Density Matrix with Gaussian Orbitals. *J. Chem. Phys.* **2001**, *114*, 9758−9763.
(74) Schlegel, H. B.; Iyengar, S. S.; Li, X.; Millam, J. M.; Voth, G. A.; Scuseria, G. E.; Frisch, M. J. Ab Initio Molecular Dynamics: Propagating the Density Matrix with Gaussian Orbitals. III. Comparison with Born−Oppenheimer Dynamics. *J. Chem. Phys.* **2002**, *117*, 8694−8704.
(75) Stewart, J. J. P. Optimization of Parameters for Semiempirical Methods V: Modification of NDDO Approximations and Application to 70 Elements. *J. Mol. Model.* **2007**, *13*, 1173−1213.
(76) Kashiwabara, T.; Takahashi, Y.; Tanimizu, M.; Usui, A. Molecular-Scale Mechanisms of Distribution and Isotopic Fractionation of Molybdenum between Seawater and Ferromanganese Oxides. *Geochim. Cosmochim. Acta* **2011**, *75*, 5762−5784.
(77) Müller, A.; Diemann, E.Thiomolybdates and Thiotungstates: Their Properties and Role as Ligands in Coordination Chemistry. *Nitrogen Fixation*; Springer: Boston, MA, 1983; pp 183−210.
(78) Gili, P.; Tsipis, A. C. Electronic Structure Calculations on Multiply Charged Anions Containing M-S Bonds (M = Cr, Mo, W) and Their Heterobimetallic Cluster Complexes. *Int. J. Quantum Chem.* **2007**, *107*, 418−439.
(79) Zhang, H.; Kim, C.-K. Hydration of Formaldehyde in Water: Insight from ONIOM Study. *Bull. Korean Chem. Soc.* **2008**, *29*, 2528−2530.
(80) Silla, E.; Arnau, A.; Tunon, I.Fundamental Principles Governing Solvent Use: Solvent Effects on Chemical Systems. *Handbook of Solvents*; ChemTec Publishing, 2003; Vol. *34*.
(81) Oyerinde, O. F.; Weeks, C. L.; Anbar, A. D.; Spiro, T. G. Solution Structure of Molybdic Acid from Raman Spectroscopy and DFT Analysis. *Inorg. Chim. Acta.* **2008**, *361*, 1000−1007.
(82) Schott, J.; Mavromatis, V.; Fujii, T.; Pearce, C. R.; Oelkers, E. H. The Control of Carbonate Mineral Mg Isotope Composition by Aqueous Speciation: Theoretical and Experimental Modeling. *Chem. Geol.* **2016**, *445*, 120−134.
(83) Dupuis, R.; Benoit, M.; Nardin, E.; Méheut, M. Fractionation of Silicon Isotopes in Liquids: The Importance of Configurational Disorder. *Chem. Geol.* **2015**, *396*, 239−254.
(84) Pinilla, C.; Blanchard, M.; Balan, E.; Natarajan, S. K.; Vuilleumier, R.; Mauri, F. Equilibrium Magnesium Isotope Fractionation between Aqueous Mg^{2+} and Carbonate Minerals: Insights from Path Integral Molecular Dynamics. *Geochim. Cosmochim. Acta* **2015**, *163*, 126−139.
(85) Kendall, B.; Dahl, T. W.; Anbar, A. D. The stable isotope geochemistry of molybdenum. *Rev. Mineral. Geochem.* **2017**, *82*, 683−732.
(86) Huerta-Diaz, M. A.; Morse, J. W. Pyritization of Trace Metals in Anoxic Marine Sediments. *Geochim. Cosmochim. Acta* **1992**, *56*, 2681−2702.
(87) Crusius, J.; Calvert, S.; Pedersen, T.; Sage, D. Rhenium and Molybdenum Enrichments in Sediments as Indicators of Oxic, Suboxic and Sulfidic Conditions of Deposition. *Earth Planet. Sci. Lett.* **1996**, *145*, 65−78.
(88) Helz, G. R.; Bura-Nakić, E.; Mikac, N.; Ciglenečki, I. New Model for Molybdenum Behavior in Euxinic Waters. *Chem. Geol.* **2011**, *284*, 323−332.
(89) Tribovillard, N.; Riboulleau, A.; Lyons, T.; Baudin, F. Enhanced Trapping of Molybdenum by Sulfurized Marine Organic Matter of Marine Origin in Mesozoic Limestones and Shales. *Chem. Geol.* **2004**, *213*, 385−401.
(90) Algeo, T. J.; Lyons, T. W. Mo−Total Organic Carbon Covariation in Modern Anoxic Marine Environments: Implications for Analysis of Paleoredox and Paleohydrographic Conditions. *Paleoceanography* **2006**, *21*, No. PA1016.
(91) Bertine, K. K.; Turekian, K. K. Molybdenum in Marine Deposits. *Geochim. Cosmochim. Acta* **1973**, *37*, 1415−1434.
(92) Scott, C.; Lyons, T. W.; Bekker, A.; Shen, Y.-A.; Poulton, S. W.; Chu, X.-L.; Anbar, A. D. Tracing the Stepwise Oxygenation of the Proterozoic Ocean. *Nature* **2008**, *452*, 456−459.
(93) Bura-Nakić, E.; Andersen, M. B.; Archer, C.; de Souza, G. F.; Marguš, M.; Vance, D. Coupled Mo-U Abundances and Isotopes in a Small Marine Euxinic Basin: Constraints on Processes in Euxinic Basins. *Geochim. Cosmochim. Acta* **2018**, *222*, 212−229.
(94) Wasylenki, L. E.; Rolfe, B. A.; Weeks, C. L.; Spiro, T. G.; Anbar, A. D. Experimental Investigation of the Effects of Temperature and Ionic Strength on Mo Isotope Fractionation during Adsorption to Manganese Oxides. *Geochim. Cosmochim. Acta* **2008**, *72*, 5997−6005.
(95) Wang, X.; Sherman, D. M. Molecular Speciation of Mo (VI) on Goethite and Its Implications for Molybdenum and Its Isotopic Cycle in Ocean. *Geochim. Cosmochim. Acta* **2021**, *313*, 116−132.
(96) Tang, H.-R.; Fan, K.-N. Application of ONIOM to Cluster Modeling of the Metal Surface. *Chem. Phys. Lett.* **2000**, *330*, 509−514.
(97) Sierraalta, A.; Añez, R.; Diaz, L.; Gomperts, R. Interaction of CO Molecule with Au/MOR Catalyst: ONIOM-PM6 Study, Active

Sites, Thermodynamic and Vibrational Frequencies. *J. Phys. Chem. A* **2010**, *114*, 6870−6878.
(98) Farrokhpour, H.; Ghandehari, M.; Eskandari, K. ONIOM DFT Study of the Adsorption of Cytosine on the Au/Ag and Ag/Au Bimetallic Nanosurfaces: The Effect of Sublayer. *Appl. Surf. Sci.* **2018**, *457*, 712−725.

https://doi.org/10.1021/acsearthspacechem.2c00268
ACS Earth Space Chem. 2023, 7, 142−155